

1 Global Greenhouse Gas Reconciliation 2022

2 Zhu Deng^{1,2,3}, Philippe Ciais^{4,*}, Liting Hu⁵, Adrien Martinez⁴, Marielle Saunois⁴, Rona L. Thompson⁶,
3 Kushal Tibrewal⁴, Wouter Peters^{7,8}, Brendan Byrne⁹, Giacomo Grassi¹⁰, Paul I. Palmer^{11,12}, Ingrid T.
4 Luijkx⁷, Zhu Liu^{1,2,3,*}, Junjie Liu^{9,13}, Xuekun Fang⁵, Tengjiao Wang¹⁴, Hanqin Tian¹⁵, Katsumasa
5 Tanaka^{4,16}, Ana Bastos¹⁷, Stephen Sitch¹⁸, Benjamin Poulter¹⁹, Clément Albergel²⁰, Aki Tsuruta²¹, Shamil
6 Maksyutov¹⁶, Rajesh Janardanan¹⁶, Yosuke Niwa^{16,22}, Bo Zheng^{23,24}, Joël Thanwerdas²⁵, Dmitry
7 Belikov²⁶, Arjo Segers²⁷, Frédéric Chevallier⁴

8 ¹Department of Geography, University of Hong Kong, Hong Kong SAR, China

9 ²Institute for Climate and Carbon Neutrality, University of Hong Kong, Hong Kong SAR, China

10 ³Department of Earth System Science, Tsinghua University, Beijing, China

11 ⁴Laboratoire des Sciences du Climat et de l'Environnement, IPSL, CEA-CNRS-UVSQ, Université Paris-Saclay, Gif-sur-
12 Yvette, France

13 ⁵College of Environmental & Resource Sciences, Zhejiang University, Hangzhou, Zhejiang, China

14 ⁶Norwegian Institute for Air Research (NILU), Kjeller, Norway

15 ⁷Meteorology and Air Quality Department, Wageningen University & Research, Wageningen, the Netherlands

16 ⁸Energy and Sustainability Research Institute Groningen, University of Groningen, Groningen, the Netherlands

17 ⁹Jet Propulsion Laboratory, California Institute of Technology, Pasadena, CA, USA

18 ¹⁰Joint Research Centre, European Commission, Ispra (VA), Italy

19 ¹¹National Centre for Earth Observation, University of Edinburgh, Edinburgh, UK

20 ¹²School of GeoSciences, University of Edinburgh, Edinburgh, UK

21 ¹³Division of Geological and Planetary Sciences, California Institute of Technology, Pasadena, CA, USA

22 ¹⁴Institute of Blue and Green Development, Shandong University, Weihai, China

23 ¹⁵International Center for Climate and Global Change Research, School of Forestry and Wildlife Sciences, Auburn University,
24 Auburn, AL 36849, USA

25 ¹⁶Earth System Division, National Institute for Environmental Studies, Onogawa 16-2, Tsukuba, Ibaraki 305-8506, Japan

26 ¹⁷Institute for Earth System Science and Remote Sensing, Leipzig University, 04103 Germany

27 ¹⁸Faculty of Environment, Science and Economy, University of Exeter, Exeter, UK

28 ¹⁹NASA Goddard Space Flight Center, Biospheric Sciences Laboratory, Greenbelt, MD 20771, USA

29 ²⁰European Space Agency Climate Office, ECSAT, Harwell Campus, Didcot, Oxfordshire, UK

30 ²¹Finnish Meteorological Institute, P.O. Box 503, 00101, Helsinki, Finland

31 ²²Department of Climate and Geochemistry Research, Meteorological Research Institute (MRI), Nagamine 1-1, Tsukuba,
32 Ibaraki 305-0052, Japan

33 ²³Shenzhen Key Laboratory of Ecological Remediation and Carbon Sequestration, Institute of Environment and Ecology,
34 Tsinghua Shenzhen International Graduate School, Tsinghua University, Shenzhen, 518055, China

35 ²⁴State Environmental Protection Key Laboratory of Sources and Control of Air Pollution Complex, Beijing 100084, China

36 ²⁵Empa, Swiss Federal Laboratories for Materials Science and Technology, Dübendorf, Switzerland

37 ²⁶Center for Environmental Remote Sensing, Chiba University, Chiba, Japan

38 ²⁷TNO, Department of Air quality and Emissions Research, P.O. Box 80015, NL-3508-TA, Utrecht, the Netherland

39 *Correspondence to:* Philippe Ciais (philippe.ciais@lsce.ipsl.fr); Zhu Liu (zhuliu@tsinghua.edu.cn)

40 **Abstract.** In this study, we provide an update of the methodology and data used by Deng et al. (2022) to compare the national
41 greenhouse gas inventories (NGHGs) and atmospheric inversion model ensembles contributed by international research teams

42 coordinated by the Global Carbon Project. The comparison framework uses transparent processing of the net ecosystem
43 exchange fluxes of carbon dioxide (CO₂) from inversions to provide estimates of terrestrial carbon stock changes over managed
44 land that can be used to evaluate NGHGs. For methane (CH₄), and nitrous oxide (N₂O), we separate anthropogenic emissions
45 from natural sources based directly on the inversion results, to make them compatible with NGHGs. Our global harmonized
46 NGHGs database was updated with inventory data until February 2023 by compiling data from periodical UNFCCC
47 inventories by Annex I countries and sporadic and less detailed emissions reports by non-Annex I countries given by National
48 Communications and Biennial Update Reports. For the inversion data, we used an ensemble of 22 global inversions produced
49 for the most recent assessments of the global budgets of CO₂, CH₄ and N₂O coordinated by the Global Carbon Project with
50 ancillary data. The CO₂ inversion ensemble in this study goes through 2021, building on our previous report from 1990 to
51 2019, and includes three new satellite inversions compared to the previous study, and an improved managed land mask. As a
52 result, although significant differences exist between the CO₂ inversion estimates, both satellite and in-situ inversions over
53 managed lands indicate that Russia and Canada had a larger land carbon sink in recent years than reported in their NGHGs,
54 while the NGHGs reported a significant upward trend of carbon sink in Russia but a downward trend in Canada. For CH₄ and
55 N₂O, the results of the new inversion ensembles are extended to 2020. Rapid increases in anthropogenic CH₄ emissions were
56 observed in developing countries, with varying levels of agreement between NGHGs and inversion results, while developed
57 countries showed a slow declining or stable trend in emissions. Much denser sampling of atmospheric CO₂ and CH₄
58 concentrations by different satellites, coordinated into a global constellation, is expected in the coming years. The methodology
59 proposed here to compare inversion results with NGHGs can be applied regularly for monitoring the effectiveness of
60 mitigation policy and progress by countries to meet the objective of their pledges. The dataset constructed for this study is
61 publicly available at <https://doi.org/10.5281/zenodo.13887128> (Deng et al., 2024).

62 **1 Introduction**

63 If modeled pathways align with Nationally Determined Contributions (NDCs) declared prior to COP26 (in 2021) until 2030
64 and do not involve any subsequent increase in ambition, the projected global warming by 2100 would be 2.1-3.4°C (IPCC,
65 2023). The global stocktake coordinated by the secretariat of the United Nations Framework Convention on Climate Change
66 (UNFCCC) considers data from national greenhouse gas inventories (NGHGs) to assess the collective climate progress to
67 curb emissions. It is expected there will be differences in the quality of NGHGs being reported to the UNFCCC (Perugini et
68 al., 2021). UNFCCC Annex I Parties, which include all OECD (Organisation for Economic Co-operation and Development)
69 countries and several EIT (Economies In Transition) already report annually their emissions following the same IPCC
70 guidelines (IPCC 2006) in a common reporting format, with a time latency of roughly 1.5 years. In contrast, non-Annex I
71 Parties, mostly developing and less developed countries, are currently not required to provide reports as regularly and as
72 detailed as Annex I Parties and in a few cases use different IPCC Guidelines in their National Communications (NC) or
73 Biennial Update Reports (BUR) submitted to the UNFCCC. Non-Annex I Parties are scheduled in 2024 to move to regular

74 and harmonized reporting of their emissions in the national inventory reports (NIRs) in the format of common reporting tables
75 (CRTs), following the Paris Agreement’s enhanced transparency framework (ETF).

76 The IPCC guidelines for NGHGs encourage countries to use independent information to verify emissions and removals
77 (IPCC, 1997, 2006, 2019), such as comparisons with independently compiled inventory databases (e.g. IEA, CDIAC, EDGAR,
78 FAOSTAT), or with atmospheric mole fraction measurements interpreted by atmospheric inversion models (see Section 6.10.2
79 in IPCC (2019)). Such verification of ‘bottom-up’ national reports against ‘top-down’ atmospheric inversion results is not
80 mandatory. However, a few countries (e.g. Switzerland, United Kingdom, New Zealand, and Australia) have already added
81 inversions as a consistency check of their national reports. In our study, we utilized the latest global inversion results from the
82 budget assessments of CO₂, CH₄, and N₂O conducted by the Global Carbon Project (GCP), focusing on three ensembles of
83 inversions with global coverage. Compared to our previous study (Deng et al., 2022), the CO₂ inversion ensemble used in this
84 study has been updated to the global CO₂ budget of Friedlingstein et al. (2022) that includes nine CO₂ inversions using mole
85 fraction data from the surface network and/or retrieval products from the Greenhouse Gases Observing Satellite (GOSAT) and
86 Orbiting Carbon Observatory-2 (OCO-2) satellites. The CH₄ inversion ensemble and N₂O inversion (Tian et al., 2023)
87 ensemble used in this study are also extended to the 2020. As a result, the new ensembles cover up to 2021 for CO₂, 2020 for
88 CH₄ and 2020 for N₂O, compared to 2019, 2017 and 2016 respectively in our previous study (Deng et al., 2022), allowing us
89 to track and analyze the most recent flux variations.

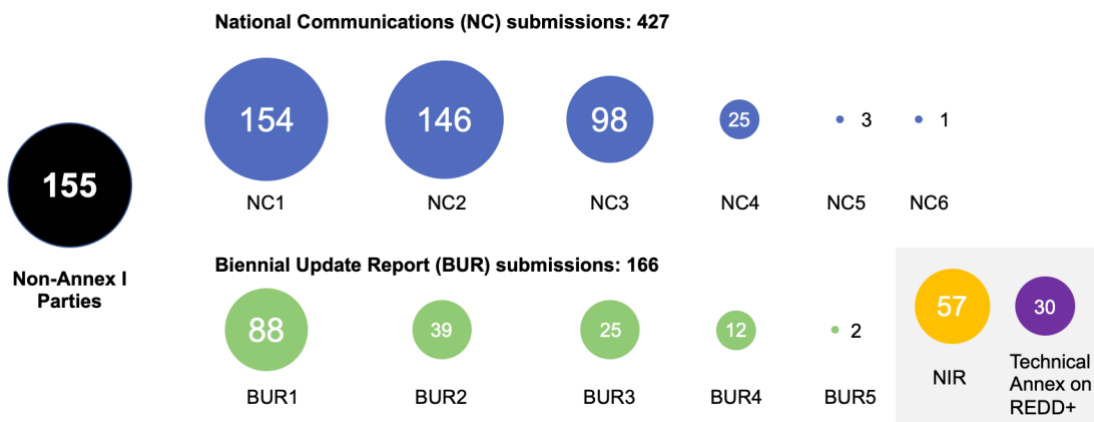
90 Our framework to process the inversion data aims at making them comparable to inventories at countries or groups of countries
91 scale (ie,with an area larger than the spatial resolution of atmospheric transport models typically used for inversions).
92 Atmospheric inversions use *a priori* information for the spatial and temporal patterns of fluxes. Some inversions correct prior
93 fluxes at the spatial resolution of their transport models to match atmospheric observations and use spatial error correlations
94 (usually e-folding length scales) that tie the adjustment of fluxes from one grid cell to its neighbors at distances of tens to
95 hundreds of kilometers. Other inversions adjust fluxes over coarse regions that are larger than the resolution of the transport
96 model, implicitly assuming a perfect correlation of flux errors within these regions, causing an aggregation error (Kaminski et
97 al., 2001). Thus, to minimize aggregation errors, the results of inversions are shown preferentially for selected large area
98 emitter countries or large absorbers in the case of CO₂. We have selected a different set of countries or groups of countries for
99 each gas, according to their importance in the global emission budget. According to the median of inversion data we used in
100 this study, selected countries collectively represent ~70% of global fossil fuel CO₂ emissions, ~90% of global land CO₂ sink,
101 ~60% of anthropogenic CH₄ emissions, and ~55% of anthropogenic N₂O emissions (Fig S1). To more robustly interpret
102 global inversion results for comparison with inventories, we follow the same criterion and choose high-emitting countries
103 covered (if possible) by atmospheric measurements, although most selected tropical countries have few or no atmospheric in-
104 situ stations. Uncertainties are given by the spread among inversion models (min-max range given the small number of
105 inversions), and the causes for discrepancies with inventories are analyzed systematically and on a case-by-case basis,
106 considering both individual countries and specific greenhouse gases, for annual variations and for mean budgets over several
107 years.

108 Based on the newly updated inversion results and inventory, and an improvement in the methodology framework proposed in
 109 the previous study (Deng et al., 2022), we specifically address the following questions: 1) how do inversion models compare
 110 with NGHGs for the three gases?; 2) what are the plausible reasons for mismatches between inversions and NGHGs?; 3) did
 111 the new maps of managed land masks in this study reduce the mismatch between the inversions and NGHGs for CO₂ and
 112 N₂O?; 4) what independent information can be extracted from inversions to evaluate the mean values or the trends of
 113 greenhouse gas emissions and removals?; 5) does this information exhibit a good agreement with NGHGs?; and 6) how do
 114 satellite-retrieval driven inversion models differ from the surface in-situ and flask sampling driven inversion model results?
 115 Sections 2 presents the updated global database of national emissions reports for selected countries and its grouping into
 116 sectors, the global atmospheric inversions used for the study, the processing of fluxes from these inversions to make their
 117 results as comparable as possible with inventories. The time series of inversions compared with inventories for each gas, with
 118 insights on key sectors for CH₄ are discussed in **Sections 3 to 5**. The discussion (Section 6) focuses on the plausible reasons
 119 for mismatches between inversions and NGHGs, comparison between inversion ensembles in this study and previous study,
 120 and different priors applied in the CH₄ inversions. Finally, concluding remarks are drawn on how inversions could be used
 121 systematically to support the evaluation and possible improvement of inventories for the Paris Agreement.

122 2 Material and methods

123 2.1 Compilation and harmonization of national inventories reported to the UNFCCC

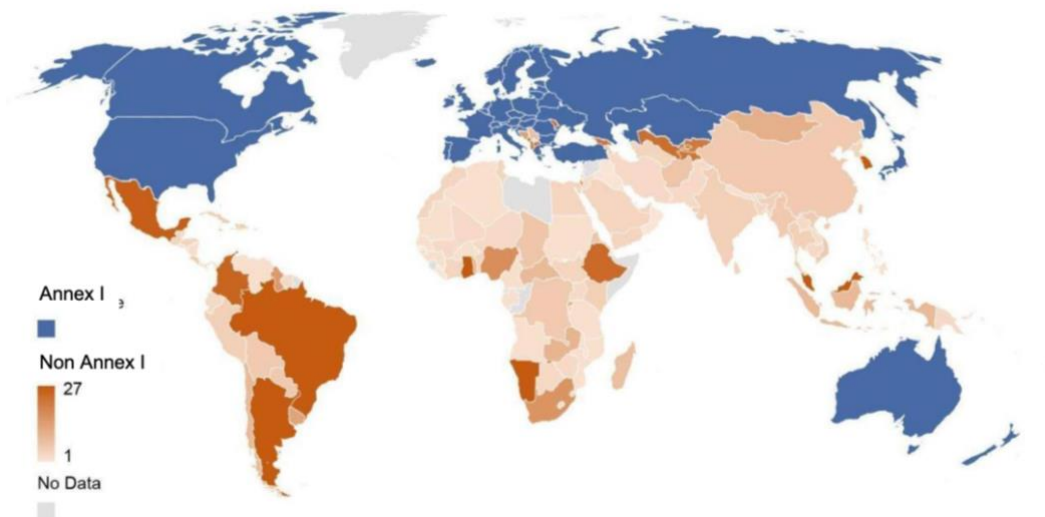
124 All UNFCCC Parties shall periodically update and submit their national GHG inventories of emissions by sources and
 125 removals by sinks to the Convention parties. Annex I countries submit their NIRs in common reporting format (CRF) tables
 126 every year with a complete time series starting in 1990. Non-Annex I Parties are required to submit their NC roughly every
 127 four years after entering the Convention and submit BUR, every two years since 2014. Currently, there are in total 427
 128 submissions of NC and over 166 submissions of BUR (UNFCCC, 2021b, a) (**Fig 1**).



129

130 **Figure 1. Numbers of non-Annex I parties for each submission round (as of February 28, 2023).** The numbers in the middle of the dots
131 denote the numbers of non-Annex I parties for each submission, while the black dots denote the total number of non-Annex I parties, the
132 blue dots denote the numbers of non-Annex I parties who has submitted National Communications (NC), green dots for Biennial Update
133 Reports (BUR), yellow dots for National Inventory Report (NIR), and purple dots for Technical Annex on REDD+ . The numbers after the
134 NC and BUR denote the total number of submission reports.

135 We collected NGHGIS data submitted to UNFCCC by February 28, 2023. For Annex I countries, data collection is
136 straightforward, as their reports are provided as Excel files under a Common Reporting Format (CRF) until the year 2020 last
137 accessed on February 28, 2023. For non-Annex I countries, the data were directly extracted from the original reports provided
138 in Portable Document Format (PDF) last accessed on February 28, 2023. Data from successive reports for the same country
139 were extracted, except when they relate to the same years, in which case only the latest version is considered. While Annex I
140 countries are required to compile their inventory following IPCC 2006 guidelines and the subdivision between sectors
141 established by the UNFCCC decision (dec. 24/CP.19), non-Annex I countries are increasingly adopting the IPCC 2006
142 Guidelines, although some still utilize the older IPCC 1996 Guidelines, with different approaches and sectors. Consequently,
143 the methods used and the reported sectors may differ among NC and BUR reports.



144 **Figure 2. Number of years covered by NGHGI reports (NC+BUR) in each non-Annex I country (as of February 28, 2023).** Emissions
145 from Greenland are reported by Denmark.
146

147 2.2 Atmospheric inversions

148 CO₂ inversions

149 Nine CO₂ inversion systems from the 2022 Global Carbon Budget of the GCP (Friedlingstein et al., 2022) are used, including
150 CarbonTracker-Europe (CTE) v2022 (van der Laan-Luijkx et al., 2017), Jena CarboScope v2022 (Rödenbeck et al., 2003), the

151 surface air-sample inversion from the Copernicus Atmosphere Monitoring Service (CAMS) v21r1 (Chevallier et al., 2005),
 152 the inversion from the CAMS Satellite FT21r2 (Chevallier et al., 2005), the inversion from the University of Edinburgh (UoE)
 153 v6.1b (Feng et al., 2016), the NICAM-based Inverse Simulation for Monitoring CO₂ (NISMON-CO₂) v2022.1 (Niwa et al.,
 154 2022), CMS-Flux v2022 (Liu et al., 2021), GONGGA v2022 (Jin et al., 2023), and THU v2022 (Kong et al., 2022). A variety
 155 of transport models are used by these systems, which allows for representing a major driver factor behind differences in flux
 156 estimates based on atmospheric inversions, particularly their distribution over latitudinal bands. Among the nine inversions,
 157 four systems (CAMS Satellite FT21r2, GONGGA v2022, THU v2022, and CMS-Flux v2022) utilize satellite CO₂ column
 158 retrievals from GOSAT and/or OCO-2, calibrated to the World Meteorological Organization (WMO) 2019 standards. CMS-
 159 Flux additionally incorporates in-situ observed CO₂ mole fraction records. The remaining five inversion systems (CAMS
 160 v21r1, CTE v2022, Jena Carboscope v2022, UoE v6.1b, and NISMON-CO₂ v2022.1) solely rely on CO₂ mole fractions that
 161 were observed in-situ or collected in flasks (Schuldt et al., 2021, 2022). The CO₂ inversion records extend up to and including
 162 2021. Their flux estimates are available at https://meta.icos-cp.eu/objects/GahdRITjT22GGmq_GCi4o_wy and details are
 163 summarized in **Table 1**.

164 **Table 1 | Atmospheric CO₂ inversions used in this study** (Friedlingstein et al., 2022)

Inversion System	Version	Period	Observation	Transport Model
CarbonTracker Europe (CTE): CTE2022_SiB4 (van der Laan-Luijkx et al., 2017)	v2022	2001-2021	Ground-based Obspack GLOBALVIEW plus v7.0 and NRT_v7.2	TM5
Jena Carboscope sEXTocNEET (Rödenbeck et al., 2003)	v2022	1960-2021		TM3
Copernicus Atmosphere Monitoring Service (CAMS) (Chevallier et al., 2005)	v21r1	1979-2021		LMDZ v6
The University of Edinburgh (UoE) (Feng et al., 2016)	v6.1b	2001-2021		GEOS-CHEM
the NICAM-based Inverse Simulation for Monitoring CO ₂ (NISMON-CO ₂) (Niwa et al., 2022)	v2022.1	1990-2021		NICAN-TM

CMS-Flux (Liu et al., 2021),	v2022	2010-2021	Ground-based & ACOS-GOSAT v9r; OCO-2 v10 scaled to WMO2019	GEOS-CHEM
CAMS-Satellite (Chevallier et al., 2005)	FT21r2	2010-2021	bias-corrected ACOS GOSAT v9 over land until August 2014 + bias- corrected ACO S OCO-2 v10 over land, both rescaled to WMO2019	LMDZ v6
THU (Kong et al., 2022)	v2022	2015-2021	OCO-2 v10r data scaled to WMO2019	GEOS-CHEM
GONGGA (Jin et al., 2023)	v2022	2015-2021	OCO-2 v10r data scaled to WMO2019	GEOS-CHEM

165 **CH₄ inversions**

166 The CH₄ emissions come from the new ensemble of inversions (Saunois et al. 2024) from 2000 to 2020, using seven different
167 inverse systems for a total nine inversions (**Table 2**). The inverse systems include: CarbonTracker-Europe CH₄ (Tsuruta et
168 al., 2017), LMDZ-PYVAR (Yin et al., 2015; Zheng et al., 2018), CIF-LMDZ(Berchet et al., 2021), MIROC4-ACTM (Patra
169 et al., 2018; Chandra et al., 2021), NISMOM-CH₄ (Niwa et al., 2022), NIES-TM-FLEXPART (Maksyutov et al., 2021;
170 Janardanan et al., 2024), and TM5-CAMS (Segers and Houweling, 2017). This ensemble of inversions gathers various
171 chemistry transport models, differing in vertical and horizontal resolutions, meteorological forcing, advection (horizontal
172 transport of air) and convection (vertical transport) schemes, and boundary layer mixing (detailed characteristics can be found
173 in Table S11 in Saunois et al. 2024). Including these different systems is a conservative approach that allows to cover different
174 potential uncertainties of the inversion, among them: model transport, set-up issues, and prior dependency. All inversions
175 except two, use updated common prior emission maps for natural and anthropogenic prior emissions divided into 12 sectors,
176 particularly the EDGAR v6 inventory for prior fossil fuel emissions (Crippa et al., 2021a extrapolated to Jan 1st, 2021), GFED
177 for fires and ecosystem models for wetland emissions. During the production of the inversion simulations, GAINS inventory
178 (Höglund-Isaksson, 2013) was proposed to use another prior for fossil fuel sources, instead of using EDGAR v6 (see
179 Supplementary Text 3 in Saunois et al, 2024). GAINS has higher fossil emissions, in particular over the US and a higher
180 increase of fossil emissions over time in the US (Tibrewal et al., 2024). As Tibrewal et al. showed that inversions are strongly
181 attracted to their priors, comparison between results with GAINS and EDGAR v6 priors is informative about how robust are
182 inversions to their priors when they are used to ‘verify’ NGHGs. Some inversions optimize emissions in groups of sectors,
183 and others only provide total gridded emissions (MIROC4-ACTM and TM5-CAMS, details can be found in Table S10 in

184 Saunois et al, 2024). For the latter, we computed the emission from each sector within each pixel based on the proportion of
 185 the prior fluxes. Such processing can lead to significant uncertainties if not all sources increase or change at the same rate in a
 186 given region/pixel. The inversions assimilating surface stations mole fraction observations provide results since 2000, and
 187 those assimilating satellite observations from column CH₄ measurements (XCH₄) of the GOSAT satellite provide results since
 188 2010, first full year of GOSAT observations. Inversion results were gridded into 1° by 1° monthly emission maps and
 189 aggregated nationally using a country mask (Klein Goldewijk et al., 2017).

190 **Table 2 | Atmospheric CH₄ inversions used in this study (Saunois et al, 2024)**

Inversion system	Abbreviation	Institution	Observations	Period
Carbon Tracker-Europe CH ₄	CTE	FMI	Surface stations	2000-2020
CIF-LMDz	CIF-LMDz	LSCE/CEA	Surface stations	2000-2020
LMDz-PYVAR	PYVAR-LMDz	LSCE/CEA	GOSAT Leicester v7.2	2010-2020
MIROC4-ACTM	MIROC4-ACTM	JAMSTEC	Surface stations	2000-2020
NISMON-CH ₄	NISMON-CH ₄	NIES/MRI	Surface stations	2000-2020
NIES-TM-FLEXPART (NTF)	NIES	NIES	Surface stations	2000-2020
NIES-TM-FLEXPART (NTF)	NIES	NIES	Surface + GOSAT NIES L2 v02.95	2010-2020
TM5-CAMS	TM5	TNO/VU	Surface stations	2000-2020

TM5-CAMS	TM5	TNO/VU	GOSAT (combined observations)	ESA/CCI with surface	v2.3.8	2010-2020
----------	-----	--------	-------------------------------------	----------------------------	--------	-----------

191 **N₂O inversions**

192 Four N₂O inversion systems from the updated GCP Nitrous Oxide Budget (Tian et al., 2023) are used: INVICAT (Wilson et
193 al., 2014), PyVAR-CAMS (Thompson et al., 2014), MIROC4-ACTM (Patra et al., 2018, 2022) and GEOS-Chem (Wells et
194 al., 2015). The N₂O inversion results are updated up to 2020.

195 **Table 3 | Atmospheric N₂O inversions used in this study** (Tian et al., 2023)

Inversion system	Institution	Period
INVICAT (Wilson et al., 2014)	Univ. Leeds	1995-2020
PyVAR-CAMS (Thompson et al., 2014),	NILU/LSCE	1995-2020
MIROC4-ACTM (Patra et al., 2018, 2022)	JAMSTEC	1997-2019
GEOS-Chem (Wells et al., 2015)	Univ. Minnesota	1995-2019

196 **Aggregating the gridded inversion results into national totals**

197 To obtain national annual-scale flux estimates, we aggregated the gridded flux maps of each inversion with various native
198 resolutions following the methodology outlined in Chevallier (2021). This involved using the 0.08° x 0.08° land country mask
199 of Klein Goldewijk et al. (2017) to calculate the fraction of each country in each inversion grid box.

200 **2.3 Processing of CO₂ inversion data for comparison with NGHGs**

201 **Fossil fuel emissions re-gridding - managed land mask**

202 To analyze terrestrial CO₂ fluxes, we subtracted the same fossil fuel emissions (including cement) of GridFEDv2022.2 (Jones
203 et al., 2022) from the total CO₂ flux of each inversion. This is equivalent to assuming perfect knowledge of fossil emissions,

204 adding up to a global total of 9.7 Gt C/yr for the year 2021. The dataset used national annual emissions estimates from the
 205 2022 global carbon budget (Friedlingstein et al., 2022) which uses the reported NGHGs data from Annex I countries and are
 206 assumed to be broadly consistent with the non-Annex I countries. This assumption may lead to underestimating the uncertainty
 207 of terrestrial CO₂ fluxes deduced from inversions.

208 As defined in the IPCC Guidelines for NGHGs (IPCC, 2006), only CO₂ emissions and removals from managed land are
 209 reported in NGHGs as a proxy for human-induced effects (direct effects and indirect effects such as CO₂ fertilization and
 210 nitrogen deposition). However, inversion models retrieve all CO₂ fluxes (due to both direct and indirect effects, plus the natural
 211 interannual variability) over all lands. We thus retained inversions' national estimates of the Net Ecosystem Exchange (NEE)
 212 CO₂ flux ($F_{ML}^{inv NEE}$) over managed lands grid cells only (ML , here defined as all land except intact forests) because the fluxes
 213 over unmanaged land are not counted by NGHGs. We use NEE from the definition of Ciais et al. (2020), representing all non-
 214 fossil CO₂ exchange fluxes between terrestrial surfaces and the atmosphere. Other work may use Net Biome Production (NBP)
 215 with a similar meaning. CO₂ fluxes over unmanaged lands were excluded from the terrestrial CO₂ flux totals that will be
 216 compared with NGHGs, proportional to their presence in each inversion grid box. The new maps of non-intact forests are
 217 compiled by Grassi et al. (2023). These maps include official country-managed forest and other managed land areas for Canada
 218 and Brazil used for their NGHGs, and the intact forest map (Potapov et al., 2017) as a substitute for unmanaged land where
 219 country-based information is not available. For Russia, we used non-intact forest maps for each province with thresholds
 220 adjusted to match the official managed land areas from Russia's NIRs, and assumed that all grasslands were managed. This
 221 approach assumes that non-intact forest areas can serve as a reasonably good proxy for managed forests reported in the
 222 NGHGs (Grassi et al., 2021, 2023). It is important to note that this approach is somewhat arbitrary, as highlighted in previous
 223 studies (Ogle et al., 2018; Chevallier, 2021; Grassi et al., 2021). However, in the absence of a machine-readable definition of
 224 managed plots in many NGHGs, there is currently no better alternative available.

225 **Adjusting CO₂ fluxes due to lateral carbon transport by crop and wood products trade and by rivers**

226 In addition to the extraction of fossil CO₂ flux and managed land CO₂ flux, there are CO₂ fluxes that are part of $F_{ML}^{inv NEE}$ but
 227 are not counted by NGHGs. These fluxes are induced by (i) soils to rivers to oceans carbon export (F_{ML}^{rivers}) which has an
 228 anthropogenic and a natural component (Regnier et al., 2013), and (ii) net anthropogenic export of crop and wood products
 229 across each country's boundary ($F_{ant}^{crop trade}$ and $F_{ant}^{wood trade}$). The magnitudes of these CO₂ fluxes are different between
 230 countries, and values from the selected countries are presented in **Fig S2**. We assume that NGHGs include CO₂ losses from
 231 fire (wildfire and prescribed fire) and other disturbances (wind, pests) and from domestic harvesting, as recommended by the
 232 IPCC reporting guidelines (IPCC, 2006, 2019) (although some countries, such as Canada and Australia exclude some
 233 emissions from these disturbances, and the subsequent removals from the same areas (Grassi et al., 2023)). The adjusted
 234 inversion NEE that can be compared with inventories, $F_{adj}^{inv NEE}$, is given by:

$$235 F_{adj}^{inv NEE} = F_{ML}^{inv NEE} - F_{ML}^{rivers} - F_{ant}^{crop trade} - F_{ant}^{wood trade} \Leftrightarrow F_{ant-nf}^{ni}, \quad (1)$$

236 where the sign \Leftrightarrow means ‘compared with’, F_{ant-nf}^{ni} is the non-fossil part of the anthropogenic CO₂ flux from NGHGs, F_{tot}^{rivers}
 237 is the sum of the natural and anthropogenic CO₂ flux on land from CO₂ fixation by plants that is leached as carbon via soils
 238 and channeled to inland waters to be exported to the ocean or to another country. All countries export river carbon, but some
 239 countries also receive river inputs, e.g., Romania receives carbon from Serbia via the Danube River. We estimated the lateral
 240 carbon export by rivers minus the imports from rivers entering each country, including dissolved organic carbon, particulate
 241 organic carbon and dissolved inorganic carbon of atmospheric origin distinguished from lithogenic, by using the data and
 242 methodology described by Ciais et al. (2021). Data are from Mayorga et al. (2010) and Hartmann et al. (2009) and follow the
 243 approach of Ciais et al. (2021) proposed for large regions. We also extracted the lateral flux by rivers over the managed land
 244 by using the same methodology as inversion CO₂ flux. Thus, in a country that only exports river carbon to the ocean, the
 245 amount of carbon exported is equivalent to an atmospheric CO₂ sink, denoted as F_{ML}^{rivers} as in eq. (1), thus ignoring burial,
 246 which is a small term. Over a country that receives carbon from rivers flowing into its territory, a small national CO₂ outgassing
 247 is produced by a fraction of this imported flux. In that case, we assumed that the fraction of outgassed to incoming river carbon
 248 is equal to the fraction of outgassed to soil-leached carbon in the RECCAP2 region to which a country belongs, estimated with
 249 data from Ciais et al. (2021).
 250 $F_{ant}^{crop\ trade}$ is the sum of CO₂ sinks and sources induced by the trade of crop products. This flux was estimated from the annual
 251 trade balance of crop commodities calculated for each country from data from the United Nations Statistics Division of the
 252 Food and Agriculture Organization (FAOSTAT) combined with the carbon content values of each commodity (Xu et al., 2021;
 253 FAO, 2024). All the traded carbon in crop commodities is assumed to be oxidized as CO₂ in one year, neglecting stock changes
 254 of products, and the fraction of carbon from crop products going to waste pools and sewage waters after consumption, thus
 255 not necessarily oxidized to atmospheric CO₂. $F_{ant}^{wood\ trade}$ is the sum of CO₂ sinks and sources induced by the trade of wood
 256 products (Zscheischler et al., 2017). Here, we followed Ciais et al. (2021) who used a bookkeeping model to calculate the
 257 fraction of domestically produced and imported carbon in wood products that are oxidized in each country during subsequent
 258 years, with product lifetimes defined by Mason Earles et al (2012) and encompassing all products (including roundwood and
 259 processed products). The underlying assumption in estimating CO₂ fluxes from wood harvest is that the emissions from
 260 domestically harvested wood, in addition to imported wood minus exported wood that is not allocated to wood product pools,
 261 are released into the atmosphere during the year of harvest. Conversely, wood allocated to wood product pools is gradually
 262 released into the atmosphere over time, based on their respective lifetimes. Domestic harvest is assumed to be balanced by an
 263 atmospheric CO₂ sink of equivalent magnitude, which is not necessarily the case given that harvest is rarely in equilibrium
 264 with forest increment, but inversions NEE will correct for this imbalance in our results, and can thus be compared with
 265 NGHGs. We included in the $F_{ant}^{crop\ trade}$ flux the emissions of CO₂ by domestic animals consuming specific crop products
 266 delivered as feed. On the other hand, emissions of CO₂ from grazing animals and the decomposition of their manure are
 267 supposed to occur in the same grid box where grass is grazed, so that the CO₂ net flux captured by an inversion is comparable

268 with grazed grasslands' carbon stock changes of inventories. Emissions of reduced carbon compounds (VOCs, CH₄, CO) are
 269 not included in this analysis (see Ciais et al. (2021) for a discussion of their importance in inversion CO₂ budgets).
 270 In summary, the purpose of the adjustment of eq. (1) is to make inversion output comparable to the NGHGs that do not include
 271 $F_{ML}^{drivers}$, $F_{ant}^{crop\ trade}$ and $F_{ant}^{wood\ trade}$. The UNFCCC accounting rules (IPCC, 2006) assume that all the harvested wood
 272 products are emitted in the territory of a country that produces them, which is equivalent to ignoring $F_{ant}^{wood\ trade}$ as a national
 273 sink or source of CO₂, hence the need to remove $F_{ant}^{wood\ trade}$ from inversion NEE. The adjusted inversion fluxes from eq. (1)
 274 depict the national CO₂ stock change which match better the carbon accounting system boundaries of UNFCCC NGHGs. In
 275 the following, we will only discuss adjusted inversion CO₂ fluxes ($F_{adj}^{inv\ NEE}$), but for simplicity call them “inversion fluxes”.

276 **2.4 Processing of CH₄ inversions for comparison with national inventories**

277 Most atmospheric inversions derive total net CH₄ emissions at the surface as it is difficult for them to disentangle overlapping
 278 emissions from different sectors at the pixel/regional scale based on atmospheric CH₄ observations only. However, five of the
 279 seven inverse systems solve for some source categories owing to different spatio-temporal distributions between the sectors.
 280 For each inversion, monthly gridded posterior flux estimates were provided at 1°x1° grid resolution for the net flux at the
 281 surface (E_{net}^{inv}), the soil uptake at the surface (E_{soil}^{inv}), the total emission at the surface (E_{tot}^{inv}) and five emitting ‘super sectors’
 282 which regroup several IPCC sectors: Agriculture & Waste (E_{AgW}^{inv}), Fossil Fuel (E_{FF}^{inv}), Biomass & Biofuel Burning (E_{BB}^{inv}),
 283 Wetlands (E_{Wet}^{inv}), and Other Natural (E_{Oth}^{inv}) emissions. Considering the soil uptake as a ‘negative source’ given separately, the
 284 following equations apply:

$$285 \quad E_{net}^{inv} = E_{tot}^{inv} + E_{soil}^{inv} = E_{AgW}^{inv} + E_{FF}^{inv} + E_{BB}^{inv} + E_{Wet}^{inv} + E_{Oth}^{inv} + E_{soil}^{inv} \quad (2)$$

286 For inversions solving for net emissions only, the partition to source sectors was created based on using a fixed ratio of sources
 287 calculated from prior flux information at the pixel scale. For inversions solving for some categories, a similar approach was
 288 used to partition the solved categories to the five aforementioned emitting sectors. Such processing can lead to significant
 289 uncertainties if not all sources increase or change at the same rate in a given region/pixel. National values have been estimated
 290 using the country land mask described in the CO₂ section, thus offshore emissions are not counted as part of inversion results
 291 unless they are in a coastal grid cell.

292 In our previous study (Deng et al., 2022), four methods were proposed to separate CH₄ anthropogenic emissions from
 293 inversions (E_{Anth}^{inv}) to compare them with national inventories (E_{Anth}^{ni}) aiming to discuss the uncertainties in anthropogenic
 294 CH₄ emissions associated with the chosen separation methods. These four methods include: (1) summing prior estimates based
 295 on inversions for anthropogenic sectors (method 1); (2) subtracting natural emissions from total fluxes (method 2); and (3)
 296 subtracting natural emissions derived from other bottom-up assessments from the total inversion flux (methods 3/1 and 3/2,
 297 differing only in the bottom-up wetland CH₄ data used). The calculations of anthropogenic emissions by each method were
 298 performed separately for GOSAT inversions and in-situ inversions. However, the uncertainty from the separation method is

299 generally much smaller than the variability between different inversion models (see Deng et al. (2022) Fig 9). Therefore, we
 300 apply only one method in this study which consists of using inversion partitioning as defined in Saunio et al. (2020):

$$301 \quad E_{Anth}^{inv} = E_{AgW}^{inv} + E_{FF}^{inv} + E_{BB}^{inv} - E_{wildfires}^{BU} \Leftrightarrow E_{Anth}^{ni} \quad (3)$$

302 This method has some uncertainties. First, the partitioning relies on prior fractions within each pixel, and second, emissions
 303 from wildfires are counted for in the Biomass and Biofuel burning (*BB*) inversion category while they are not necessarily
 304 reported in NGHGs. The *BB* inversion category includes methane emissions from wildfires in forests, savannahs, grasslands,
 305 peats, agricultural residues, and the burning of biofuels in the residential sector (stoves, boilers, fireplaces). Therefore, we
 306 subtracted bottom-up (*BU*) emissions from wildfires ($E_{wildfires}^{BU}$) based on the GFEDv4 dataset (van Wees et al., 2022) using
 307 their reported dry matter burned and CH₄ emission factors. Because the GFEDv4 dataset also reports specific agricultural and
 308 waste fire emissions data, we assumed that those fires (on managed lands) are reported by NGHGs, so they were not counted
 309 in $E_{wildfires}^{BU}$. Figure S3 presents a comparison between our adjusted *BB* flux and the wood fuel emissions reported by Flammini
 310 et al. (2023). This comparison highlights the broader scope and definition of our adjusted *BB* flux, illustrating the differences
 311 in emissions estimation methodologies.

312 **2.5 Processing of N₂O inversions for comparison with inventories**

313 We subtracted estimates of natural N₂O sources from the N₂O emission budget (E_{tot}^{inv}) of each inversion, to provide inversions
 314 of anthropogenic emissions (E_{ant}^{inv}) that can be compared with national inventories (E_{ant}^{ni}):

$$315 \quad E_{ant}^{inv} = E_{ML}^{inv} - E_{nat}^{aq} - E_{wildfires}^{GFED} \Leftrightarrow E_{ant}^{ni} \quad (4)$$

316 Here, the natural N₂O sources include natural emission from freshwater systems (E_{nat}^{aq}) and natural emissions from wildfires
 317 (E_{ant}^{ni}).

318 In our previous study, intact forest grid cells (assumed unmanaged) from Potapov et al. (2017) and lightly grazed grassland
 319 areas from Chang et al. (2021) were removed from the gridded N₂O emissions in proportion to their presence in each inversion
 320 grid box. Here we used the new managed land mask defined in **Section 2.3** to filter gridded N₂O emissions from inversions to
 321 obtain E_{ML}^{inv} . We verified that the inversion grid box fractions classified as unmanaged do not contain point source emissions
 322 from the industry, energy, and diffuse emissions from the waste sector, to make sure that we do not inadvertently remove
 323 anthropogenic sources by masking unmanaged pixels. From the EDGARv4.3.2 inventory (Janssens-Maenhout et al., 2019),
 324 we found that N₂O from wastewater handling covers a relatively large area that might be partly located in unmanaged land.
 325 But the corresponding emission rates are more than 1 order of magnitude smaller than those from agricultural soils. For other
 326 sectors, only very few of the unmanaged grid boxes contain point sources, and none of them have an emission rate that is
 327 comparable with agricultural soils (managed land). Thus, our assumption that emissions from these other anthropogenic sectors
 328 are primarily over managed land pixels is solid (other sectors include: the power industry; oil refineries and transformation
 329 industry; combustion for manufacturing; aviation; road transportation no resuspension; railways, pipelines, off-road transport;

330 shipping; energy for buildings; chemical processes; solvents and products use; solid waste incineration; wastewater handling;
331 solid waste landfills).

332 The flux E_{nat}^{aq} is the natural emission from freshwater systems given by a gridded simulation of the DLEM model (Yao et al.,
333 2019) describing pre-industrial N₂O emissions from N leached by soils and lost to the atmosphere by rivers in the absence of
334 anthropogenic perturbations (considered as the average of 1900-1910). Natural emissions from lakes were estimated only at a
335 global scale by Tian et al. (2020), and represent a small fraction of rivers' emissions. Therefore, they are neglected in this
336 study. The flux $E_{wildfires}^{GFED}$ is based on the GFED4s dataset (van Wees et al., 2022) using their reported dry matter burned and
337 N₂O emission factors. Because the GFED dataset reports specific agricultural and waste fire emissions data, we assume that
338 those fires (on managed lands) are reported by NGHGs so they were not counted in $E_{wildfires}^{GFED}$ just like for CH₄ emissions.
339 Note that there could also be a background natural N₂O emission from natural soils over managed lands ($E_{managed\ land}^{soil}$) which
340 is not necessarily reported by NGHGs. We did not try to subtract this flux from managed land emissions because we assumed
341 that, after a land use change from natural to fertilized agricultural land, background emissions decrease and become very small
342 compared to N-fertilizers induced anthropogenic emissions. In a future study, we could use for $E_{managed\ land}^{soil}$ the estimate
343 given by simulations of pre-industrial N₂O emissions from the NMIP ensemble of dynamic vegetation models with carbon-
344 nitrogen interactions (number of models; n = 7). Namely, their simulation S0 in which climate forcing is recycled from 1901-
345 1920; CO₂ is at the level of 1860, and no anthropogenic nitrogen is added to terrestrial ecosystems (Tian et al., 2019).
346 Another important point to ensure a rigorous comparison between inversion and NGHGI data is whether anthropogenic indirect
347 emissions (AIE) of N₂O are reported in NGHGI reports. This is not always the case even though UNFCCC parties are required
348 to report these in their NGHGs according to the IPCC guidelines. For example, South Africa's BUR3 did not report indirect
349 N₂O emissions due to the lack of activity data. AIE arise from anthropogenic nitrogen from fertilizers leached to rivers and
350 anthropogenic nitrogen deposited from the atmosphere to soils. AIEs represent typically 20% of direct anthropogenic emissions
351 and cannot be ignored in a comparison with inversions. For Annex I countries, AIEs are systematically reported, generally
352 based on emission factors since these fluxes cannot be directly measured, and we assumed that indirect emissions only occur
353 on managed land. For non-Annex I countries, we checked manually from the original NC and BUR documents if AIE was
354 reported or not by each non-Annex I country. If AIEs were reported by a country, they were used as such to compare NGHGI
355 data with inversion results, and grouped into the agricultural sector. If they were not reported, or if their values were outside
356 plausible ranges, AIE were independently estimated by the perturbation simulation of N fertilizers leaching, CO₂ and climate
357 on rivers and lakes fluxes in the DLEM model (Yao et al., 2019), and by the perturbation simulation of atmospheric nitrogen
358 deposition on N₂O fluxes from the NMIP model ensemble (Tian et al., 2019).

359 **2.6 Grouping sectors for comparison**

360 The bottom-up NGHGs are compiled based on activity data (statistics) following the IPCC 1996/2006 Guidelines (IPCC,
361 1997, 2006) with detailed information on subsectors. However, the top-down inversions can only distinguish between very

362 few groups of sectors at most. Thus, in this study, we aggregated NGHGI sectors into some ‘super sectors’ to make inversions
 363 and inventories comparable for each GHG (**Table 2**). For CO₂, the inversions are divided into two aggregated super-sectors:
 364 fossil fuel and cement CO₂ emissions, and adjusted net land flux. Inversions use a prior gridded fossil fuel dataset as
 365 summarized in **Section 1.2**, thus, in this study, we compare only the net land flux between inversions and inventories. To
 366 calculate the net land flux over managed lands from NGHGIs, we subtracted fossil emissions from the IPCC/CRF *1. Energy*
 367 and *2. Industrial Processes* (or *2. Industrial Processes and Product Use*) sectors from the *Total GHG emissions including*
 368 *LULUCF/LUCF* (or *Total national emissions and removals*) sector. For CH₄, we compare inversions and inventories based on
 369 three super sectors, including *Fossil, Agriculture and Waste*, and *Total Anthropogenic*. To compare with NGHGIs, we group
 370 the IPCC/CRF sectors of *1. Energy* and *2. Industrial Processes* (or *2. Industrial Processes and Product Use*) by excluding
 371 Biofuel Burning (reported under *1. Energy* sector) into the super sector of *Fossil*; we group sectors of *4. Agriculture* (or *3.*
 372 *Agriculture*) and *6. Waste* (or *5. Waste*) into the super sector of *Agriculture and Waste*; and we aggregate anthropogenic flux
 373 from *Fossil* and *Agriculture and Waste* and *Biofuel Burning* into *Anthropogenic*. For N₂O, we grouped the NGHGI sectors
 374 into *Anthropogenic* flux being the sum of *1. Energy + 2. Industrial Processes* (or *2. Industrial Processes and Product Use*) +
 375 *4. Agriculture* (or *3. Agriculture*) + *6. Waste* (or *5. Waste*) + *Anthropogenic Indirect Emissions*.

376 **Table 2. Grouping of NGHGIs sectors into aggregated ‘super-sectors’ for comparisons with inversions.** * Biofuel burning is likely not
 377 included in NGHGIs but under *1.A.4 Other Sectors* if it is reported. ** Field burning of agricultural residues is reported in Annex I countries
 378 under the Agricultural sector. Note that indirect N₂O emissions are reported by Annex I countries but not systematically by non-Annex I
 379 ones

Gas	Super-Sectors	Inversions	NGHGIs (IPCC/CRF)
CO ₂	<i>Net Land Flux (adjusted)</i>	<i>Total - Fossil - lateral C</i>	Non-Annex I (IPCC): <i>Total GHG emissions including LULUCF/LUCF - (Energy + Industrial Processes)</i> Annex I (CRF): <i>Total national emissions and removals) - (Energy + Industrial Processes and Product Use)</i>
CH ₄	<i>Anthropogenic</i>	<i>Fossil + Agriculture & Waste + Biofuel Burning</i>	Energy + Industrial Processes + Agriculture + Waste + Biofuel Burning*
	<i>Fossil</i>	<i>Fossil</i>	Energy + Industrial Processes - Biofuel Burning*

<i>Agriculture and Waste</i>	<i>Agriculture & Waste</i>	Agriculture + Waste - Field burning of agricultural residues**
------------------------------	--------------------------------	--

N ₂ O	<i>Anthropogenic</i>	Total - pre-industrial inland waters	Agriculture + Waste direct + anthropogenic indirect emissions (AIE = anthropogenic N leached to inland waters + anthropogenic N deposited from atmosphere) + energy and industry
------------------	----------------------	--------------------------------------	--

380 **2.7 Choice of example countries for analysis**

381 For the analysis, we selected 12 countries (or groups of countries) based on specific criteria for each aggregated sector. Firstly,
 382 each chosen country had to possess a sufficiently large land area, as the limitations of coarse-spatial-resolution inversions
 383 make it difficult to reliably estimate GHG budgets for smaller countries. Additionally, it was preferable for the selected
 384 countries to have some coverage provided by the in situ global network of monitoring stations.

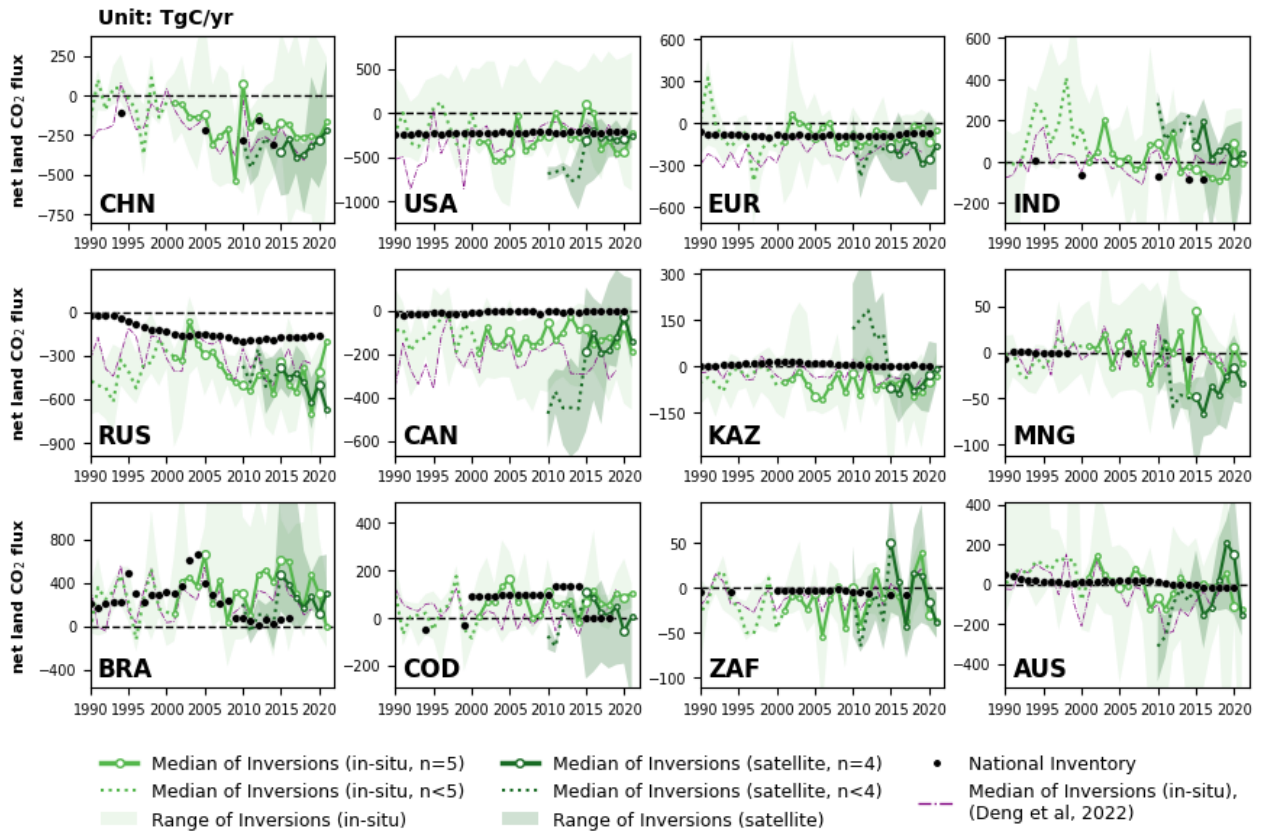
385 For CO₂, we focus on the land CO₂ fluxes of large fossil fuel CO₂ emitters. Although inversions do not allow to verify fossil
 386 emissions in these countries as they are used as a fixed prior map of emissions, it is crucial to compare the magnitude of
 387 national land CO₂ sinks with fossil fuel CO₂ emissions in those large emitters. It is important to note that fitting net fluxes to
 388 changes in atmospheric CO₂ and then subtracting the prior fossil fuel (FF) fluxes can result in errors in the residual values,
 389 which are typically attributed exclusively to the sum of all non-FF fluxes. Additionally, we included two large boreal forested
 390 countries (Russia - RUS and Canada - CAN), two tropical countries with large forest areas (Brazil - BRA and the Democratic
 391 Republic of Congo - COD), two large countries with ground-based stations (Mongolia - MNG and Kazakhstan - KAZ), and
 392 two large dry Southern Hemisphere countries also with high rankings in fossil fuel CO₂ emissions (South Africa - ZAF and
 393 Australia - AUS), both of which possess atmospheric stations to constrain their land CO₂ flux.

394 For CH₄, we first ranked countries (or groups of countries) based on their total anthropogenic, fossil, and agricultural emissions.
 395 This study includes China (CHN), India (IND), the United States (USA), the European Union (EUR), Russia (RUS), Argentina
 396 (ARG) and Indonesia (IDN), all of which are among the top emitters of both fossil fuel and agricultural CH₄ and possess large
 397 areas. Criteria of large land areas and the presence of atmospheric stations is crucial for in situ inversions. The advantage of
 398 utilizing GOSAT in CH₄ atmospheric inversions is its ability to provide observations over countries where surface in-situ data
 399 are sparse or absent, such as in the tropics. This allows us to consider countries with limited or few ground-based observations.
 400 Small countries were excluded due to the coarse spatial resolution. However, among the selected countries, Venezuela, with
 401 an area of 916,400 km², was chosen specifically for the analysis of CH₄ emissions. Despite being relatively small, Venezuela
 402 is a large producer of oil and gas, potentially allowing for inversions using GOSAT satellite observations to constrain its
 403 emissions. In major oil- and gas-extracting countries that have negligible agricultural and wetland emissions like Kazakhstan

404 (KAZ), grouped in this study with Turkmenistan (TKM) into KAZ&TKM; Iran (IRN); and Persian Gulf countries (GULF),
 405 fossil emissions should be easier to separate by inversions and thus to be compared with NGHGs.
 406 For N₂O, we selected the top 12 emitters based on the NGHGs reports. Anthropogenic N₂O emissions in most of these
 407 countries are predominantly driven by the agricultural sector, which accounts for a share (including indirect emissions) ranging
 408 from 6% in Venezuela (VEN) to 95% in Brazil (BRA) of their total NGHGs emissions.
 409 Together, the selected countries (or groups of countries) with a different selection for each gas, account for more than 90% of
 410 the global land CO₂ sink, 60% of the global anthropogenic CH₄ emissions (around 15% of fossil fuel emissions and
 411 approximately 40% of agriculture and waste emissions separately), and 55% of the global anthropogenic N₂O emissions, as
 412 estimated by the NGHGs.

413 **Table 3. Lists of countries or groups of countries are analyzed and displayed in the result section for each aggregated sector.**
 414 Argentina (ARG), Australia (AUS), BRA (Brazil), Bangladesh (BGD), Canada (CAN), China (CHN), Columbia (COL), Democratic
 415 Republic of the Congo (COD), Indonesia (IDN), India (IND), Iran (IRN), European Union (EUR), Kazakhstan (KAZ), Mexico (MEX),
 416 Mongolia (MNG), Nigeria (NGA), Pakistan (PAK), Russia (RUS), South Africa (ZAF), Sudan (SDN), Thailand (THA), United States
 417 (USA), Venezuela (VEN), GULF = Saudi Arabia + Oman + United Arab Emirates + Kuwait + Bahrain + Iraq + Qatar, KAZ&TKM =
 418 Kazakhstan + Turkmenistan. For CH₄, acronyms underlined denotes the countries appear in both *Anthropogenic* and *Fossil* or *Agriculture*
 419 *and Waste* sectors.

Gas	Super Sector	Country List
CO ₂	<i>Net Land Flux</i>	AUS, BRA, CAN, CHN, COD, EUR, IND, KAZ, MNG, RUS, USA, ZAF
CH ₄	<i>Anthropogenic</i>	<u>ARG</u> , AUS, <u>BRA</u> , <u>CHN</u> , <u>EUR</u> , <u>IDN</u> , <u>IND</u> , <u>IRN</u> , <u>MEX</u> , <u>PAK</u> , <u>RUS</u> , <u>USA</u>
	<i>Fossil</i>	<u>CHN</u> , <u>EUR</u> , GULF, <u>IDN</u> , <u>IND</u> , <u>IRN</u> , KAZ&TKM, <u>MEX</u> , NGA, <u>RUS</u> , <u>USA</u> , VEN
	<i>Agriculture and Waste</i>	<u>ARG</u> , BGD, <u>BRA</u> , <u>CHN</u> , <u>EUR</u> , <u>IDN</u> , <u>IND</u> , <u>MEX</u> , <u>PAK</u> , <u>RUS</u> , THA, <u>USA</u>
N ₂ O	<i>Anthropogenic</i>	AUS, BRA, CHN, COD, COL, EUR, IDN, IND, MEX, SDN, USA, VEN



421

422 Figure 3 | Net land CO₂ fluxes (unit: Tg C yr⁻¹) during 1990-2021 from China (CHN), United States (USA), European Union
 423 (EUR), Russia (RUS), Canada (CAN), Kazakhstan (KAZ), Mongolia (MNG), India (IND), Brazil (BRA), Democratic
 424 Republic of the Congo (COD), South Africa (ZAF), and Australia (AUS). By convention, CO₂ removals from the atmosphere
 425 are counted negatively, while CO₂ emissions are counted positively. The black dots denote the reported values from NGHGs.
 426 The light green color denotes the in-situ-alone CO₂ inversion (n=5) set while the dark green color denotes the set that uses
 427 satellite data (n=4). The green lines denote the median of land fluxes over managed land of CO₂ inversions, after adjustment
 428 of CO₂ fluxes from lateral transport by rivers, crop, and wood trade. When all inverse models within the inversion sets (in-
 429 situ: n=5; satellite: n=4) have available data for the same time interval, their median values are depicted as solid green lines.
 430 Otherwise, when the inversion sets have incomplete inverse models within the time interval (in-situ: n<5; satellite: n<4), their
 431 median values are represented as dashed green lines. Besides, before 2015, only GOSAT was available for the 2 of 4 satellite-
 432 based inversions, until September 2014 when the OCO-2 record started. The shading area denotes the min-max range of
 433 inversions. The purple dashed lines denote the median of inversions presented by the previous study (Deng et al., 2022).

434

435 **Fig 3** presents the time series of land-to-atmosphere CO₂ fluxes for the selected countries listed in **Table 2**. The median of
436 inversions across the 12 countries shows significant interannual variability, reflecting the impact of climate variability on
437 terrestrial carbon fluxes and annual variations of land-use emissions. In this paper, for inversion results covering a time interval,
438 we present the data as mean ± standard deviation, where the mean is the multi-year average of the median flux values from the
439 inversion models, and the standard deviation represents the interannual variability.

440 The adjustments of lateral CO₂ flux generally tend to lower land carbon sinks or increase land carbon emissions, especially in
441 China (CHN), United States (USA), European Union (EUR), Russia (RUS), Canada (CAN), India (IND), and Brazil (BRA).
442 In these countries, adjusting inversions by CO₂ fluxes induced by river carbon transport and by the trade of crop and wood
443 products tends to lower CO₂ sinks, especially for large crop exporters like the USA and CAN. The adjusted net lateral transport
444 fluxes for these countries are 48 (CHN), 143 (USA), 86 (EUR), 63 (RUS), 72 (CAN), 75 (IND), and 145 (BRA) Tg C/yr,
445 which represent 20%, 38%, 48%, 11%, 41%, 94%, and 60% of the managed land CO₂ fluxes before lateral transport
446 adjustments, respectively. However, even with these adjustments, in countries of temperate latitudes, the median values of the
447 five in-situ-alone inversion ensemble all indicate a net carbon sink during the 2010s, such as CHN with a sink of 180 ± 100
448 Tg C/yr, USA (210 ± 180 Tg C/yr), EUR (90 ± 50 Tg C/yr), RUS (490 ± 100 Tg C/yr) and CAN (110 ± 40 Tg C/yr). In CHN,
449 despite only 5 reported values to UNFCCC, NGHGIs show a good agreement with the inversion results, with both NGHGIs
450 and inversions exhibiting an overall increase in carbon sink over the study period. However, during 2015-2021, the median
451 values of the satellite-based inversion ensemble show a higher carbon sink of 320 ± 60 Tg C/yr than those from in-situ inversion
452 results (220 ± 50 Tg C/yr) in CHN. In IND, there are also only five reported estimates from the NGHGIs. The in-situ inversion
453 results indicate that India exhibited fluctuations between being a carbon source and a carbon sink during the period of 2001-
454 2014 (40 ± 70 Tg C/yr). During 2015-2019, the in-situ inversion results in IND show a median carbon sink of 65 ± 20 Tg C/yr,
455 however, the median reverted to being a carbon source of 90 Tg C/yr (ranging from a sink of 350 to a source of 260) in 2020.
456 In contrast, the median values of satellite-based inversion ensemble indicate a carbon source of 65 ± 64 Tg C/yr during 2015-
457 2021 in IND.

458 As Annex I countries, USA, EUR, RUS, CAN, and Kazakhstan (KAZ) have continuously reported annual NGHGIs since
459 1990. The NGHGIs reported values for the USA and CAN indicate a decline trend (Mann-Kendall Z=-0.6, p<0.01) of carbon
460 sinks by an annual average rate of 0.7 Tg C/yr² and 0.5 Tg C/yr². Like in Deng et al. 2022, we found that the carbon sink of
461 Canada's managed land is significantly larger (-130 ± 50 Tg C/yr over 2001-2021 from in-situ inversions) than the NGHGIs
462 reports (5 ± 4 Tg C/yr over 2001-2021). Part of this difference could be due to the fact that Canada decides in its inventory not
463 to report fire emissions as they are considered to have a natural cause. Doing so, Canada also excludes recovery sinks after
464 burning and those recovery sinks could surpass on average fire emissions, although remote sensing estimates of post fire
465 biomass changes suggest that fire emissions have exceeded regrowth on average in Western Canada and Alaska until ≈ 2010
466 (Wang et al., 2021). One reason for the difference may be that the NGHGI used old growth curves for forests, potentially
467 underestimating the actual forest growth. Another reason for the difference may be shrubland and natural peatland carbon
468 uptake and possibly an underestimated increase of soil carbon in the national inventory. For the USA we have a good agreement

469 between inversions (-290 ± 180 Tg C/yr for in-situ over 2001-2021) and the NGHGs data (-220 ± 10 Tg C/yr over 2001-2021)
470 with the inversion showing much more interannual variability, the US being a net source of carbon in the years 2011, 2015
471 and 2016 from the median of in-situ inversions. The lower variability in the NGHGs data reflects the 5-years averaging of C
472 stock changes by the national forest inventory. In EUR, the new in-situ inversion ensemble gives a lower carbon sink than the
473 previous one (red line in **Fig 3**, see discussion in section 6.1), now being in good agreement (-80 ± 60 Tg C/yr) with NGHGs
474 (-85 ± 10 Tg C/yr) over 2001-2021. The OCO-2 satellite inversions give a higher sink than in-situ inversions by -200 ± 80 Tg
475 C/yr, possibly because the in-situ surface network does not cover Eastern European countries which have a larger NEE than
476 Western European ones, whereas OCO-2 data have a more even coverage of the continent, as discussed by Winkler et al.
477 (2023) (see their Fig. 2 showing that OCO-2 inversions have a similar NEE than in-situ ones in Western Europe but a larger
478 mean NEE uptake in Eastern Europe).

479 In contrast, the NGHGs in RUS reports a rapid trend of increasing sink by a rate of 4.6 Tg C/yr² (Mann-Kendall $Z=0.69$,
480 $p<0.01$) during 1990-2020, supported by the significant strong correlation with the medians of in-situ inversion ensemble
481 ($\rho=0.7$, $p<0.01$) during 2001-2020. However, the median values for both the in-situ (480 ± 100 Tg C/yr) and satellite-based
482 (450 ± 90 Tg C/yr) inversion ensemble over RUS indicate larger larger land carbon sinks than those reported in the NGHGs
483 (180 ± 10 Tg C/yr) during 2011-2020. For KAZ, the NGHGs suggest that managed land is a slight carbon source (6 ± 5 Tg
484 C/yr) during 2000-2020. However, the median values for both satellite-based and in-situ inversion ensemble indicate a carbon
485 sink of 50 ± 30 Tg C/yr and 60 ± 30 Tg C/yr, respectively, during 2015-2021 and 2001-2021. It is worth noting that the
486 satellite-based inversion results for USA, CAN, and KAZ all exhibit shifts in their fluxes between 2010 and 2015 compared
487 to the results after 2015. This is attributed to the use of different satellite data and the number of different ensembles during
488 these periods. Before 2015, only GOSAT was available, and only 2 out of 4 systems were available. After the OCO-2 record
489 started, in September 2014, the satellite-driven inversion set only assimilated OCO-2. This indicates that inversion results
490 based on GOSAT data are not consistent at the country scale with OCO-2 inversions. As a result, we can compare OCO-2
491 inversions with NGHGs since 2015, but not the trends from inversions using GOSAT and/or OCO-2 inversions since 2009.
492 In BRA, both the NGHGs reports (240 ± 170 Tg C/yr during 1990-2016) and inversion results (in-situ: 350 ± 190 Tg C/yr
493 during 2001-2021; satellite-based: 280 ± 120 Tg C/yr during 2015-2021) indicate that the country has been a net carbon source
494 since 1990. The carbon source from managed land in Brazil increased from the late 1990s, reaching a peak around 2005
495 according to NGHGs (677 Tg C/yr). This evolution is confirmed by in-situ inversions with a source peaking in 2005 (~ 650
496 Tg C/yr). The net carbon source from inversions then decreased from 2005 to 2011, which is consistent with the observed
497 reduction in deforestation due to forest protection policies implemented by the Brazilian government. This is an encouraging
498 result as the inversions did not explicitly consider land use emissions in their prior assumptions, although some included an
499 estimate of carbon released by fires in their prior which is part of land-use emissions in Brazil. Since NEE is defined as all
500 land fluxes except fossil fuel emissions, NEE from all inversions nevertheless include land use emissions from deforestation,
501 degradation emissions and fire emissions including fires from deforestation, degradation and other fires. After 2011, inversions
502 show a new increase in land emissions, with a peak during the 2015-2016 El Niño. There have been higher average land

503 emissions thereafter. These ongoing changes may be attributed to various factors such as the legacy effects of drought leading
504 to increased tree mortality (Aragão et al., 2018), higher wildfire emissions (Naus et al., 2022; Gatti et al., 2023), carbon losses
505 from forest degradation, and climate change-induced reductions in forest growth due to regional drying and warming in the
506 southern and eastern parts of the Amazon (Gatti et al., 2021). From 2011 to 2016, the NGHGI reports indicate that carbon
507 emissions from Brazilian managed lands were stable at around 47 Tg C/yr. However, the medians of in-situ inversions suggest
508 that carbon emissions rapidly increased from ~100 Tg C/yr in 2011 to ~600 Tg C/yr in 2016, which peaked in 2015 (~610 Tg
509 C/yr). From 2016 to 2021, the medians for both in-situ and satellite inversion results show a decrease in carbon emissions from
510 2016 to 2018 but a transient peak in 2019, a year with large fires (Gatti et al., 2023) (in-situ: 480 Tg C/yr; satellite: 270 Tg
511 C/yr). Then carbon emissions decreased again until 2021, which experienced wetter conditions and fewer fires (Peng et al.,
512 2022); The in-situ inversion results show a continuous decrease to -10 Tg C/yr in 2021, while the satellite inversion results
513 showed a persistent source carbon anomaly of 300 Tg C/yr. We emphasize moreover that available CO₂ observations from a
514 network of aircraft vertical sampling (Gatti et al., 2021) were not used to constrain the inverse models used here.

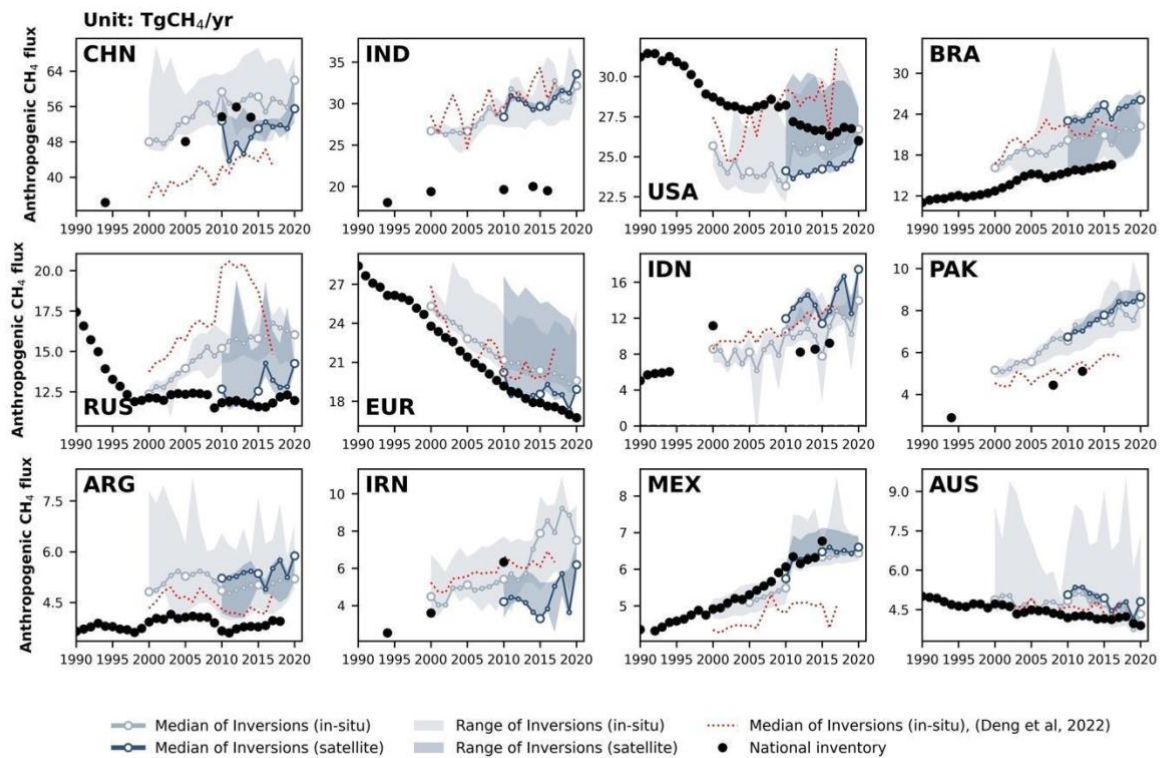
515 For Democratic Republic of the Congo (COD), the available NGHGI data indicates that before 2000, the country's managed
516 lands were a net carbon sink (50 Tg C/yr in 1994 and 30 Tg C/yr in 1999). Since 2000, the NGHGI reports indicated three
517 stages of different levels of CO₂ flux, which COD managed land was a carbon source during 2000-2010 (~95 Tg C/yr), a larger
518 carbon source during 2011-2014 (~135 Tg C/yr), and a very small sink during 2015-2018 (~-1 Tg C/yr). The medians of in-
519 situ inversion ensemble indicate a similar annual average carbon source (70 ± 45 Tg C/yr) during 2001-2021 with the NGHGI,
520 despite the few observations over Africa (Byrne et al., 2023). In the recent decade, satellite inversion results from 2015 to 2021
521 indicate a smaller source (30 ± 55 Tg C/yr) compared to the in-situ results (85 ± 25 Tg C/yr). Moreover, the satellite inversion
522 results indicate a sink anomaly in 2020 (-60 Tg C/yr) which is not found in the in-situ inversions. The sink anomaly in 2020
523 from the satellite inversions is consistent with wetter conditions during that year over COD.

524 For South Africa (ZAF), the NGHGI show a stable very small sink of 3 Tg C/yr during 1990-2010 that doubled from 4 Tg
525 C/yr in 2010 to 8 Tg C/yr in 2017, while the in-situ inversion results indicate large fluctuations from a carbon sink (especially
526 peaked in 2006, 2009, 2011, 2017 and 2021) to a small carbon source (e.g., in 2013, and 2018-2019). From 2015 to 2021, the
527 satellite-based inversion results are consistent with the in-situ results for annual variability ($\rho=0.8$, $p<0.05$), which is a good
528 sign of the consistency between different atmospheric observing systems. During the transition to El Niño conditions and
529 drought from 2014 to 2015, however, the satellite-based inversion results indicate a switch from a carbon sink to a source
530 anomaly of 50 Tg C/yr in ZAF which is not seen in the in-situ inversions.

531 In Australia (AUS), the NGHGI data shows a land source of carbon from 1990 to 2012, which decreased over time (from 48
532 Tg C/yr in 1990 to 1 Tg C/yr in 2012) and changed into a carbon sink since 2013 (that increased from a sink of 1 Tg C/yr in
533 2013 to 15 Tg C/yr in 2020). However, the in-situ inversions indicate fluctuations between a carbon source and a sink with an
534 annual average small sink of 10 ± 71 Tg C/yr observed over the period of 2001-2021, except for 2009-2011, the medians of
535 in-situ inversions reveal a strong carbon sink of 105 ± 35 Tg C/yr. Between 2010 and the strong La Niña year of 2011, the
536 medians of in-situ inversion ensemble from the previous study (Deng et al., 2022) showed an increase in carbon uptake of

537 145%. This high carbon sink persisted in 2012, which was a dryer year with maximum bushfire activity. However, in this
538 study, the medians of updated in-situ inversion ensemble indicate that there is a sink anomaly in 2011 followed by a source
539 anomaly in 2013, which appears to be more realistic. 2019 was the driest and hottest year recorded in Australia, including
540 extreme fires at the end of 2019 (Byrne et al., 2021). As a result, the medians for both in-situ and satellite inversion ensemble
541 show a carbon source anomaly in 2019, with 55 Tg C/yr (ranging from a sink of 1060 to a source of 480) and 200 Tg C/yr
542 (ranging from a sink of 120 to a source of 320) respectively. When it comes to the wet La Niña year of 2021, the medians for
543 both in-situ and satellite inversion ensemble indicate that AUS managed land became a carbon sink of 130 Tg C/yr (ranging
544 from a sink of 1120 to a source of 25) and 150 Tg C/yr (ranging from a sink of 260 to a source of 40).

545 Last, we give the global comparison between NGHGs and inversions, using NGHGs data compiled for all countries by Grassi
546 et al. (2023) which include Annex I countries reports, non-Annex I NC, BUR and NDCs. The river correction is the only one
547 that changes the global NEE, because the global mean of CO₂ fluxes from wood and crop products is close to zero. The river-
548 induced CO₂ uptake over land that is removed from inversion NEE is equal to the C flux transported to the ocean at river
549 mouths (0.9 GtC/yr in our estimate, close to the value of Regnier et al. 2022). The (in-situ) inversions without the river
550 correction give a global NEE sink of 1.8 GtC/yr over 2001-2020, managed land: 1.3 GtC/yr (72% of total), unmanaged land:
551 0.5 GtC/yr (28%). The in-situ inversions with the river correction study give a global NEE sink of 0.91 GtC/yr, managed land
552 0.51 GtC/yr (56% of total), unmanaged land 0.4 GtC/yr (44% of the total). This is an important update from Deng et al. 2022
553 where the river CO₂ flux correction was not applied separately to managed / unmanaged lands. Because managed lands have
554 a much larger area than unmanaged ones and because of the spatial patterns of the CO₂ sinks in the river correction are
555 distributed with MODIS NPP which has low values in unmanaged lands of northern Canada and Russia, the river correction
556 reduces strongly the C storage change with respect to NEE over managed lands, and marginally in unmanaged lands. Inventory
557 data recently compiled by Grassi et al. (2023) indicates a similar global land sink (on managed land) of 0.53 GtC yr⁻¹ with gap-
558 filled data during the same period than the inversions with our improved river correction.



561
 562 **Figure 4. Total anthropogenic CH₄ fluxes for the 12 top emitters: China (CHN), India (IND), United States (USA), Brazil (BRA),**
 563 **Russia (RUS), European Union (EUR), Indonesia (IDN), Pakistan (PAK), Argentina (ARG), Iran (IRN), Mexico (MEX), and**
 564 **Australia (AUS).** The black dots denote the reported values from NGHGIS. The light and dark blue lines/areas denote the median and
 565 maximum-minimum ranges of in-situ and satellite-based CH₄ inversions based on EDGARv6.0 as the prior respectively.

566
 567 **Fig 4** presents the variations in anthropogenic CH₄ emissions for the 12 selected countries, where these emissions are summing
 568 the sectors of agriculture and waste, fossil fuels, and biofuel burning. The distribution of emissions is highly skewed even
 569 among the top 12 emitters, with the largest and most populated countries such as China (CHN), India (IND), United States
 570 (USA), Brazil (BRA), Russia (RUS), and European Union (EUR) which emits more than 10 Tg CH₄/yr annually, while other
 571 countries have smaller emissions (ranging from 3 to 10 CH₄/yr) that are more challenging to quantify through inversions.
 572 During 2010-2020, CHN has the highest total anthropogenic emissions at around 50 ± 4 Tg CH₄/yr, followed by IND with
 573 30 ± 1 Tg CH₄/yr, USA with 24 ± 1 Tg CH₄/yr, BRA with 24 ± 1 Tg CH₄/yr, EUR with 19 ± 1 Tg CH₄/yr,
 574 Indonesia (IDN) with 14 ± 1 Tg CH₄/yr and RUS with 13 ± 1 Tg CH₄/yr, according to the medians of satellite-based
 575 inversion ensemble based on EDGARv6.0 as prior. The remaining countries have emissions of approximately 5 Tg CH₄/yr. In

576 general, the difference between NGHGs and inversions aligns in the same direction based on both satellite and in-situ
577 inversions. This provides some confidence for using inversions to evaluate NGHGs as the satellite observations are
578 independent from in situ networks. Overall, satellite-based inversions may be more robust across most countries due to better
579 observation coverage, except in EUR and the USA where the in-situ network is more extensive.

580 Developing countries, such as CHN, IND, BRA, IDN, Pakistan (PAK), Iran (IRN) and Mexico (MEX), show a rapid increase
581 in anthropogenic CH₄ emissions supported by reported values from NGHGs and results from inversions. In CHN, the reported
582 values from NGHGs (when available) generally align with the results obtained through inversions (e.g., during 2010-2015,
583 NGHGs: 54 ± 1 Tg CH₄/yr, in-situ: 58 ± 1 Tg CH₄/yr, satellite-based: 48 ± 3 Tg CH₄/yr). During 2010-2020, the median
584 values for the in-situ and satellite-based inversion ensemble show a similar increase trend at an annual growth rate of 0.28 Tg
585 CH₄/yr² and 0.26 Tg CH₄/yr² respectively, although the medians of in-situ inversion ensemble (58 ± 2 Tg CH₄/yr) were slight
586 higher than the satellite-based ensemble (50 ± 3 Tg CH₄/yr). However, in 2020, the medians of the emission estimates for both
587 in-situ and satellite-based inversions reveal a rapid increase by 9% and 11% compared to 2019 in CHN, indicating a possible
588 surge in anthropogenic methane emissions for that year, possibly an artifact from the fact that the decreased OH sink in 2020
589 is not well accounted for here. Indeed OH interannual variability were not prescribed to all inversions, and when accounted
590 for the OH interannual variability prescribed (based on Patra et al., 2021) was much smaller than those suggested by recent
591 studies (e.g., Peng et al., 2022). As a result overestimating the sink in the inversions leads to overestimated surface emissions.
592 The surge in emissions could also be due to spin-down, the last six month to one year of inversions being less constrained by
593 the observations, even though the inversion period covered up to June 2021.

594 In IND, PAK and MEX, there is good agreement ($r > 0.8$, $p < 0.01$) between the in-situ and satellite-based inversion ensembles
595 (respectively, 31 ± 1 Tg CH₄/yr and 30 ± 1 Tg CH₄/yr in IND, 8 ± 1 Tg CH₄/yr and 7 ± 1 Tg CH₄/yr in PAK, and 6 ± 1 Tg
596 CH₄/yr and 6 ± 1 Tg CH₄/yr in MEX), while both of them present a significant increasing trend of anthropogenic methane
597 emissions in these countries (Mann-Kendall $p < 0.05$). However, when comparing to NGHGs values, the inversion results in
598 IND and PAK indicate $> 50\%$ larger emissions than the values reported from the NGHGs during 2010-2020. In contrast,
599 values reported from the NGHGs (~ 6 Tg CH₄/yr) by MEX also show good agreement with the inversion results.

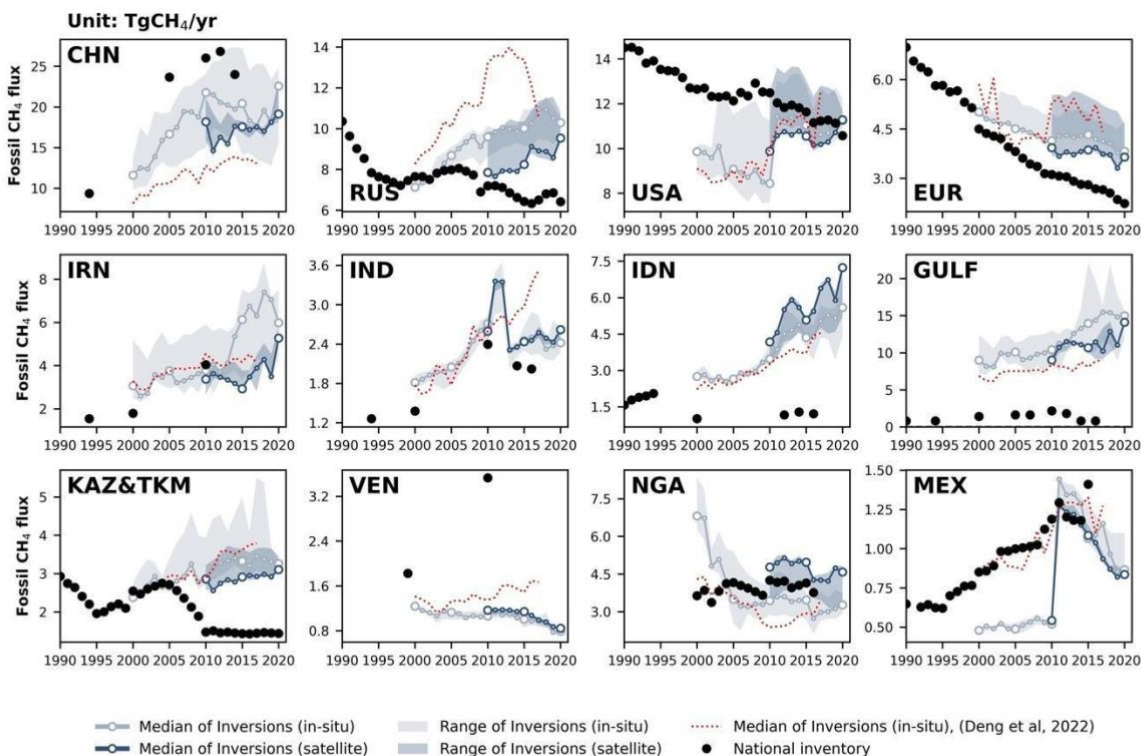
600 In BRA, IDN and Argentina (ARG), the medians for in-situ and satellite-based inversion ensembles show good consistency
601 ($r = 0.8$, $p < 0.01$) in these two countries, while satellite-based inversion results are generally higher than the in-situ inversion
602 results. Specifically, in BRA, the satellite-based inversions (24 ± 1 Tg CH₄/yr) were 16% higher than the in-situ inversions (21
603 ± 1 Tg CH₄/yr) and 52% higher than the NGHGs estimation (~ 17 Tg CH₄/yr) during 2010-2020, possibly owing to difficulties
604 for inversions to separate between natural (wetlands, inland waters) and anthropogenic sources in this country, and possible
605 flaws in the prior used for natural and anthropogenic fluxes. In IDN, NGHGs reported a significant continuous upward trend
606 at an annual average growth of 0.3 Tg CH₄/yr, with a noticeable positive outlier in 2000. The medians for both in-situ and
607 satellite-based inversion ensembles also indicate an upward trend in IDN, but both of them present sudden dips in
608 anthropogenic methane emissions in 2015 and 2019 by 15~23% and 16~25%, compared to the previous year respectively. It
609 is unlikely that anthropogenic activities could contribute such large year to year variations except for different flooded areas

610 used for rice paddies. In ARG, the satellite-based inversion results also indicate two sudden dips in 2016 and 2019, however,
611 such pattern was not found in the in-situ inversion results. A cause of year to year variations from inversions is the lack of in-
612 situ sites and variable cloud cover affecting the density of GOSAT data.

613 Regarding IRN, NGHGs only provided data for three years (1994, 2000, and 2010), making it difficult to compare with
614 inversion results. However, NGHGs show a rapid growth in anthropogenic CH₄ emissions (+9.4%/yr) during this period.
615 There are significant differences between inversion results and for IRN, with satellite inversions generally giving lower
616 emissions than in-situ inversions and different trends. Satellite inversions suggest a declining trend between 2010 and 2015,
617 followed by a fluctuating increase until 2020. In contrast, in-situ-based inversions (by any nearby measurement stations, thus
618 likely reflecting the prior trend) show a rapid rise in emissions after 2010, reaching a peak in 2018, followed by a decline.

619 NGHGs for RUS indicate that anthropogenic CH₄ emissions have been reduced during the 1990s and remained stable since
620 2000 (12.0 ± 0.3 Tg CH₄/yr during 2000-2020), which is similar with the trend observed from satellite-based inversion results
621 (12.7 ± 0.9 Tg CH₄/yr during 2000-2020). However, in 2016, there was a sudden increase of emissions in satellite inversion
622 results (+14% increase from 12.5 Tg CH₄/yr in 2015 to 14.2 Tg CH₄/yr in 2016), followed by a gradual decline, and then a
623 new increase in 2020 (+11% increase from 12.8 Tg CH₄/yr in 2019 to 14.3 Tg CH₄/yr in 2020). This recent change was not
624 observed in the in-situ inversion results or the NGHGs.

625 For USA, Australia (AUS), and EUR, NGHGs reported a slow declining trend (EUR: 0.4 Tg CH₄/yr; USA: 0.2 Tg CH₄/yr;
626 AUS: -0.04 Tg CH₄/yr) in anthropogenic CH₄ emissions. In the case of the USA, inversion-derived emissions are slightly
627 lower than NGHGs (in-situ-based: 9% lower during 2000-2020; satellite-based: 11% lower during 2010-2020). However,
628 both ground-based and satellite-based inversions indicate that anthropogenic CH₄ emissions have remained relatively steady
629 since 2000, without reflecting the slow decline reported by NGHGs. In EUR, NGHGs indicate that anthropogenic CH₄
630 emissions have been decreasing rapidly since 1990 (-1.4%/yr), consistent with the trend obtained from inversion results.
631 However, in-situ inversion emissions are on average slightly higher than NGHGs, and this difference has been gradually
632 increasing from 8% in the 2000s to 15% in the 2010s.



634

635 **Figure 5.** CH₄ emissions from the fossil fuel sector from the top 12 emitters of this sector: China (CHN), Russia (RUS), United States
 636 (USA), European Union (EUR), Iran (IRN), India (IND), Indonesia (IDN), Persian Gulf countries (GULF = Saudi Arabia + Iraq +
 637 Kuwait + Oman + United Arab Emirates + Bahrain + Qatar), Kazakhstan & Turkmenistan (KAZ&TKM), Venezuela (VEN),
 638 Nigeria (NGA), and Mexico (MEX). The black dots denote the reported value from the NGHGs. In the NGHGI data shown in Fig 5 for
 639 GULF, Saudi Arabia reported four NGHGs in 1990, 2000, 2010, and 2012, Iraq reported one in 1997, Kuwait reported three in 1994, 2000,
 640 and 2016, Oman reported one in 1994, United Arab Emirates reported four in 1994, 2000, 2005 and 2014, Bahrain reported three in 1994,
 641 2000 and 2006, and Qatar reported one in 2007. The reported values are interpolated over the study period to be summed up and plotted in
 642 the figure. For KAZ&TKM, the reported values of Turkmenistan during 2001-2003, 2005-2009, 2011-2020 are interpolated and added to
 643 annual reports from Kazakhstan, an Annex I country for which annual data are available. Other lines, colors and symbols as **Fig 4**.

644

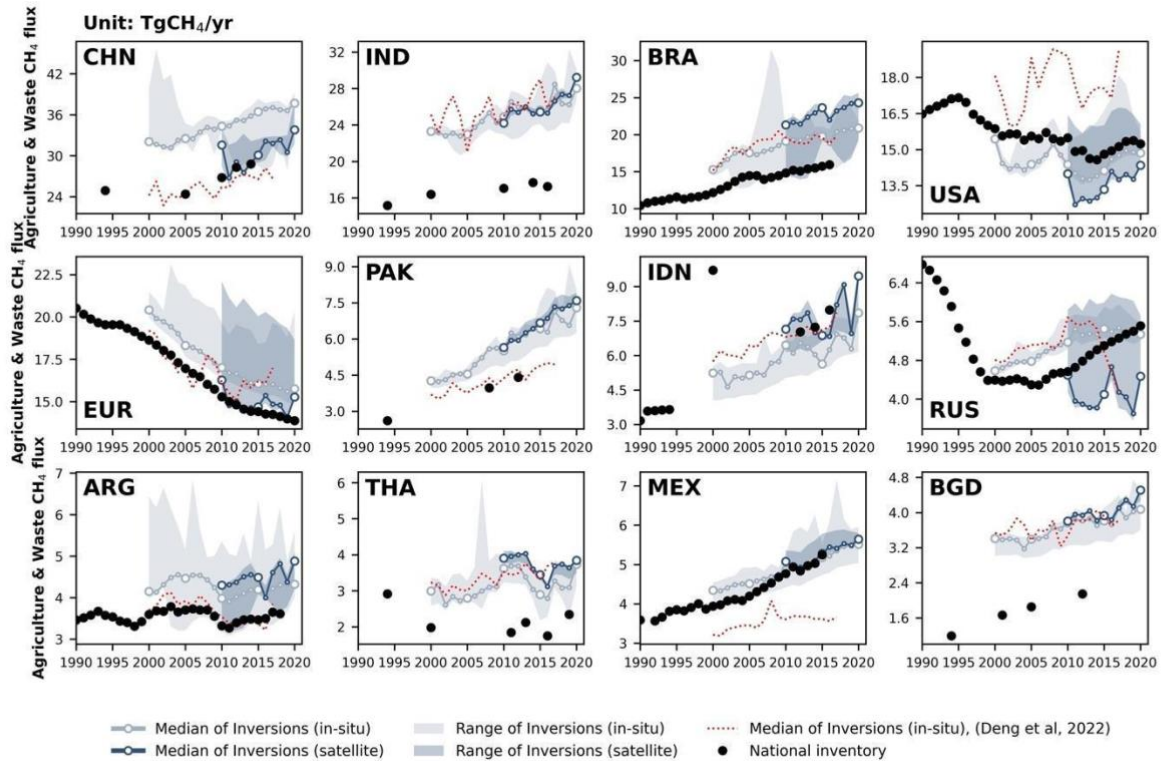
645 **Fig 5** presents the fossil CH₄ emissions for the top 12 emitters from the fossil sector based on EDGARv6.0 as the prior. The
 646 largest emitter is China (CHN), mainly from the sub-sector of coal extraction, followed by Russia (RUS) and the United States
 647 (USA). In CHN, the in-situ (20 ± 2 Tg CH₄/yr) and satellite inversions (17 ± 1 Tg CH₄/yr) emissions in the 2010s are 24% and
 648 35% lower than in the NGHGs (~ 26 Tg CH₄/yr), respectively. The NGHGs in CHN suggest a decrease from 28 in 2012 to
 649 24 Tg CH₄/yr in 2014. However, both in-situ and satellite inversion results indicate an increasing trend since 2018. In India
 650 (IND) and Indonesia (IDN), NGHGs report a decreasing trend during the study period, while inversions suggest a rapid

651 increase in IDN and a stable value in IND after a peak in 2012. In IND, satellite inversions suggest a peak of fossil CH₄
652 emissions during 2011-2012, which then dropped in 2013 and remained stable afterward. In IDN, both in-situ and satellite
653 inversions indicate a fluctuating trend, with a significant drop between 2015 and 2019. In RUS, both in-situ and satellite
654 inversion-based estimates of fossil fuel emissions are higher than NGHGs, and show an increasing trend, while NGHGs
655 report a decreasing trend. This discrepancy may be due to inversion problems for separating between wetland emissions and
656 gas extraction industries both located in the Yamal peninsula area, or leaks not captured in NGHGs. In USA, NGHGs overall
657 show a significant declining trend (Mann-Kendall Z=-0.8, p<0.01). In-situ inversion estimates of fossil fuel emissions are 26%
658 lower than NGHGs during 2000-2010, and remained consistent until around 2011. Nearly all in-situ inversions show a jump
659 in fossil fuel emissions in 2011. In the European Union (EUR), both NGHGs and inversion results demonstrate a consistent
660 declining trend. However, starting from 2010, both in-situ and satellite inversions are higher than NGHGs reports.

661 Major oil-producing countries in the Persian Gulf are too small compared to the model resolution to be studied individually.
662 Hence, NGHGs from the GULF countries (Saudi Arabia, Iraq, Kuwait, Oman, United Arab Emirates, Bahrain, and Qatar)
663 were grouped and show much lower emissions compared to inversion results. In the 2010s, in-situ and satellite inversions
664 estimate that emissions in GULF were 9 times and 8 times higher than the estimates reported in NGHGs, respectively. This
665 huge under-reporting of emissions in GULF could be partly attributed to the omission of ultra-emitters in NGHGs. The ultra-
666 emitters defined by Lauvaux et al. (2022) are namely all short-duration leaks from oil and gas facilities (e.g., wells,
667 compressors) with an individual emission >20 t CH₄/h, each event lasting generally less than one day. Such leaks are often
668 random occurrences and difficult to quantify, which is why most countries do not account for these significant and episodic
669 events in the national inventories. Indeed, recent studies by Lauvaux et al. (2022) have identified more ultra-emitters and larger
670 emission budgets from ultra-emitters in Qatar, Kuwait, and Iraq. In KAZ&TKM, grouped together because of their rather small
671 individual areas, both in-situ (3 ± 0.2 Tg CH₄/yr) and satellite (3 ± 0.1 Tg CH₄/yr) inversions estimate emissions to be 2 times
672 higher than NGHGs (1.5 Tg CH₄/yr) in the 2010s. Similarly, KAZ is located downwind of TKM, which has a high share of
673 ultra-emitters. The global inversions operating at a coarse resolution may misallocate emissions from TKM to KAZ. It is worth
674 noting that KAZ has two in-situ stations for CH₄ measurements, whereas the GULF countries lack in-situ station networks.
675 On the other hand, the GOSAT satellite provides a dense sampling of atmospheric column CH₄ in the Persian Gulf region due
676 to frequent cloud-free conditions. Therefore, GOSAT inversions can be considered more accurate than in-situ inversions for
677 Iran (IRN), GULF countries, and Kazakhstan & Turkmenistan (KAZ&TKM). Additionally, it is important to note that GOSAT
678 inversions generally give lower emissions than in-situ inversions in those countries. Venezuela (VEN) is a rare case where
679 NGHGs report much higher CH₄ emissions than inversions. While the uncertainty of GOSAT inversions (model spread) has
680 decreased compared to the results reported by Deng et al. 2022, the gap between inversions and NGHGs has increased. In
681 2010, NGHGs reports of fossil CH₄ emissions in VEN were 298% higher than GOSAT inversions and 326% than in-situ
682 inversions. We do not have a clear explanation for this large difference, except that VEN has strongly decreased oil and gas
683 extraction due to sanctions curbing its crude production from 2.7 mb/d in 2015 to 0.6 mb/d in 2020 (OPEC, 2023), which may
684 not be reflected in their NGHGs. In Nigeria (NGA) and Mexico (MEX), NGHGs estimates fall between the median of in-

685 situ and satellite inversions during 2010-2020. However, in MEX, the in-situ inversion was 50% lower than NGHGs in the
 686 2000s and showed a sudden large increase in 2010.

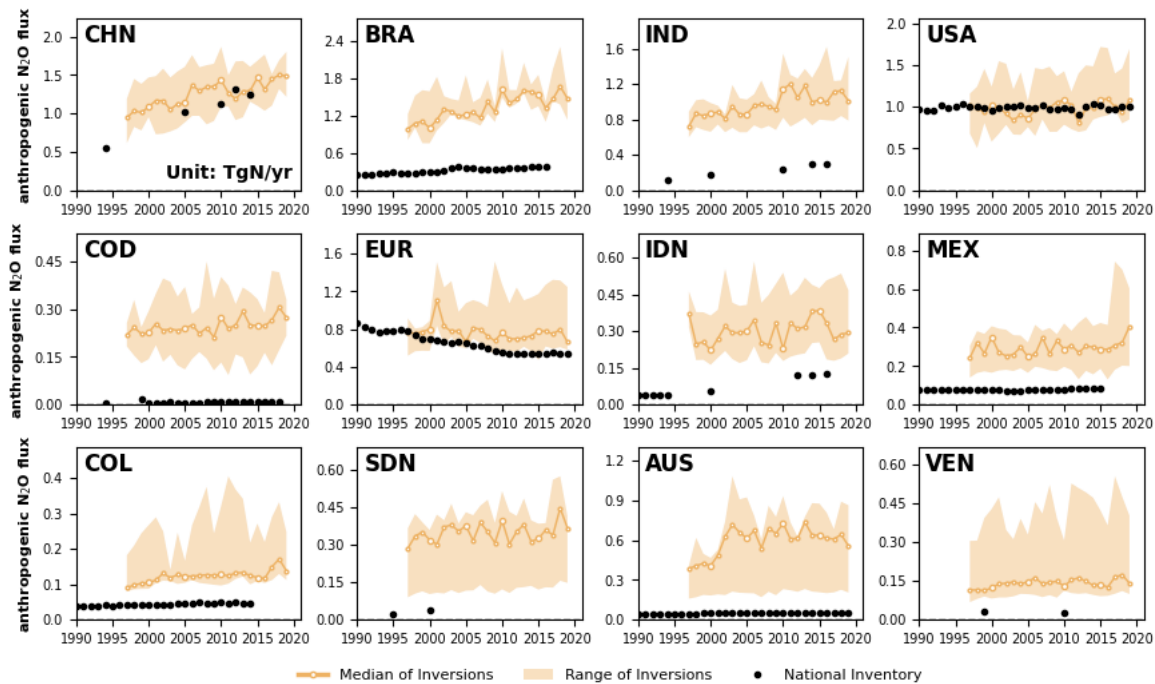
687 **4.3 Agriculture and waste CH₄ emissions**



688
 689 **Figure 6.** CH₄ emissions from agriculture and waste for the 12 largest emitters in this sector, China (CHN), India (IND), Brazil
 690 (BRA), United States (USA), European Union (EUR), Pakistan (PAK), Indonesia (IDN), Russia (RUS), Argentina (ARG), Thailand
 691 (THA), Mexico (MEX), and Bangladesh (BGD). The black dots denote the reported estimates from NGHGs. Other lines, colors, and
 692 symbols as Fig 4.

693
 694 **Fig 6** presents CH₄ emissions of the Agriculture and Waste sector for the top 12 emitters of this sector. In all countries except
 695 for the United States (USA) and Russia (RUS), the values reported by NGHGs are systematically lower than the inversion
 696 results. The results from the previous ensemble of in-situ inversions (red dotted line) are consistent with those of the inversions
 697 used in this study except in the USA where previous inversions are 3.2 Tg CH₄/yr higher, in RUS where they show a drop
 698 after 2015 although they remain in the range from the new satellite and in-situ inversions, and in Mexico (MEX) where they
 699 are systematically lower by 1.6 Tg CH₄/yr.

700 In China (CHN), the most recent NGHGI reports in 2012 and 2014 estimate agriculture and waste emissions at 28 Tg CH₄/yr,
701 which is close to satellite inversions (28 ± 1 Tg CH₄/yr) but 22.4% lower than the median in-situ inversions (35 ± 1 Tg CH₄/yr)
702 and closer to their minimum value. The trend in agricultural and waste emissions is consistent between inversions and NGHGIs
703 for CHN. In India (IND), inversions consistently show higher emissions than NGHGIs by approximately 50% and indicate an
704 increasing trend during 2000-2020, whereas the NGHGI last communication being for 2016, it does not allow us to give a
705 recent trend. According to the national inventory of IND, enteric fermentation is the primary source of CH₄ emissions in the
706 agriculture and waste sector, contributing 61% of emissions, with rice cultivation accounting for 20% and waste contributing
707 16%. A similar pattern is observed in Bangladesh (BGD), where agricultural emissions are dominated by rice production (48%
708 in 2012) and enteric fermentation (42% in 2012). Satellite and in-situ inversions estimate emissions in BGD are nearly double
709 than those reported by NGHGIs during 2001 and 2012, the last communication. The significant discrepancies between
710 inversions and NGHGIs in IND and BGD may be attributed to potential underestimation of livestock or waste CH₄ emissions
711 by NGHGIs. NGHGIs utilized the Tier 1 method and associated emission factors from the 2006 IPCC Guidelines for National
712 Greenhouse Gas Inventories (IPCC, 2006). However, a recent study (Chang et al., 2021) found that estimates using revised
713 Tier 1 or Tier 2 methods from the 2019 Refinement to the 2006 IPCC Guidelines for National Greenhouse Gas Inventories
714 (IPCC, 2019) give livestock emissions 48%-60% and 42%-61% higher for IND and BGD by 2010, respectively, compared to
715 Tier 1 IPCC (2006) methods, which would bring bottom up emissions closer to inversions. In Brazil (BRA), both satellite and
716 in-situ inversions consistently estimate larger emissions than the NGHGIs by 34% and 29%, respectively, and show a
717 consistent increasing trend over their study periods. In the USA, the medians of satellite and in-situ inversions are slightly
718 lower than those of NGHGIs, but they exhibit a similar trend throughout the study period. The trend of inversions is comparable
719 to the one of the NGHGIs in BRA during their period of overlap, although there is no NGHGIs communication later than 2016.
720 In Argentina (ARG), Pakistan (PAK) and Thailand (THA), the medians of in-situ inversions show good consistency with
721 satellite inversion results. Nevertheless, in-situ inversion emissions in the 2010s are, on average, 47% higher in PAK, 20%
722 higher in ARG, and 64% higher in THA compared to the NGHGIs reports. In European Union (EUR), emissions from
723 agriculture and waste were reported to have significantly decreased over time in the NGHGI data, mainly from solid waste
724 disposal (Petrescu et al., 2021), a trend that is captured by inversions and is close to the one of the NGHGIs over the study
725 period. In contrast, emissions from agriculture and waste in RUS are reported to have a positive trend after 2010 by the NGHGI,
726 with in-situ inversions producing a consistent trend from 2000 to 2014 but a sharp decrease thereafter, while satellite inversions
727 are producing stable emissions, albeit lower than the NGHGIs and in-situ inversions after 2010.



729

730

Figure 7. Anthropogenic N₂O fluxes of the top 12 emitters: China (CHN), Brazil (BRA), India (IND), United States (USA), Democratic Republic of the Congo (COD), European Union (EUA), Indonesia (IDN), Mexico (MEX), Colombia (COL), Sudan (SDN), Australia (AUS), and Venezuela (VEN). The black dots denote the anthropogenic emissions from the UNFCCC national greenhouse gas inventories. The thick orange lines and the light orange areas denote the median and the maximum-minimum ranges of anthropogenic fluxes respectively among all N₂O inversions. We restricted our analysis to data starting from 1997 because it was the year when data from the all four inversion models are available.

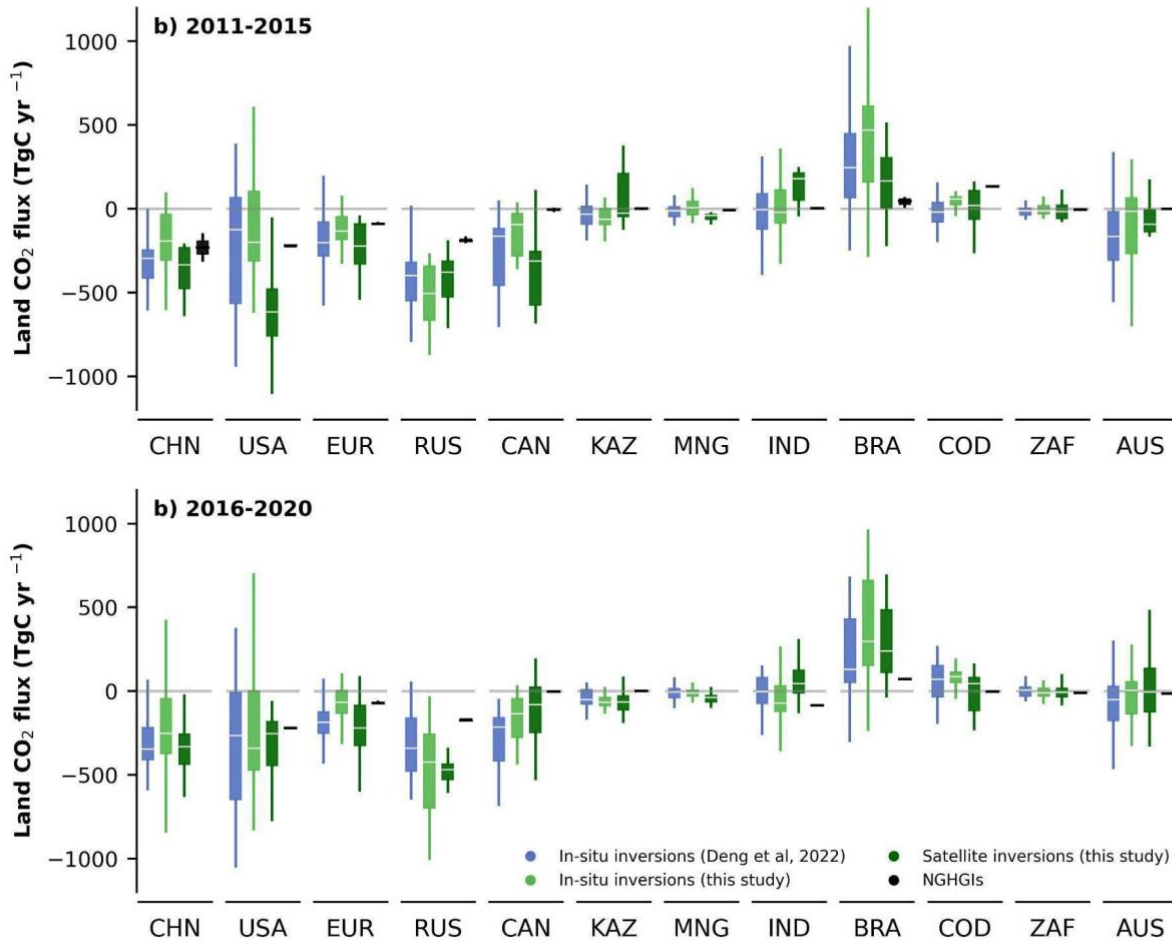
736

737

We present the 12 countries/regions with the largest anthropogenic N₂O emissions in the world (**Fig 7**), which in total contribute approximately 55% of global anthropogenic N₂O emissions. The estimates from both NGHGs and inversions in China (CHN), United States (USA), and European Union (EUR) demonstrate a relatively close match between NGHGs and inversions (in-situ only). These three large emitting countries/regions exhibit different trends in their anthropogenic N₂O emissions. In CHN, both NGHGs and inversions indicate an increasing trend in anthropogenic N₂O emissions. In the USA, anthropogenic N₂O emissions seem to have reached a state of relative stability, with NGHGs and inversion results showing similar mean values and lack of trends. In EUR, both NGHGs and inversions show a declining trend in anthropogenic N₂O emissions, but from 2010 to 2020, the NGHGs estimates are lower (20%) than the median values derived from inversion models, that is, the negative trend from inversions is less pronounced than the one of NGHGs. Most other selected countries display higher anthropogenic N₂O emissions from inversions than from NGHGs (i.e., Brazil (BRA), India (IND), Democratic

746

747 Republic of the Congo (COD), Indonesia (IDN), Mexico (MEX), Colombia (COL), Sudan (SDN), Venezuela (VEN)). These
748 discrepancies in anthropogenic N₂O emissions are possibly attributable to factors that have been analyzed in our previous study
749 (Deng et al., 2022). Firstly, nearly all these non-Annex 1 countries utilize Tier 1 emission factors (EFs), which may
750 underestimate emissions when soil and climate dependence are taken into account (Cui et al., 2021). This has been noted in
751 previous studies (Philibert et al., 2013; Shcherbak et al., 2014; Wang et al., 2020). Furthermore, the observed concave response
752 of cropland soil emissions as a function of added N fertilizers may also contribute to underestimated emissions in NGHGs, as
753 the relationship is non-linear and higher than the linear relation used by NGHGs in Tier 1 approaches (Zhou et al., 2015). In
754 an improved reporting framework, EFs should also account for both natural and anthropogenic components, as they cannot be
755 distinguished through field measurements, from which EFs are derived. However, in practice, EFs are mostly based on
756 measurements made in temperate climates and soils from established croplands with few "background" emissions.
757 Consequently, there could be a systematic underestimation of default IPCC EFs from tropical climates and for recently
758 established agricultural lands, for which the IPCC EFs also have a huge uncertainty of up to $\pm 75\%$ –100%. Another factor that
759 might contribute to the discrepancy is the omission of emissions from reactive nitrogen contained in organic fertilizers
760 (manure), for which NGHGs do not provide specific details for non-Annex 1 reports. Lastly, anthropogenic indirect emissions
761 (AIEs) from atmospheric nitrogen deposition and leaching of human-induced nitrogen additions to aquifers and inland waters
762 are reported by Annex 1 countries using simple emission factors, but non-Annex 1 countries do not consistently report AIE.
763 However, in Australia (AUS), the gap between inversions and NGHGs has even expanded compared to our previous study.
764 We do acknowledge that the density of the N₂O in-situ network in tropical countries and around AUS is so low that inversions
765 most likely are attracted to their priors. The use of a lower prior could thus also be consistent with scarce atmospheric
766 observations, and we have only a low confidence on N₂O inversion results for tropical countries and AUS.



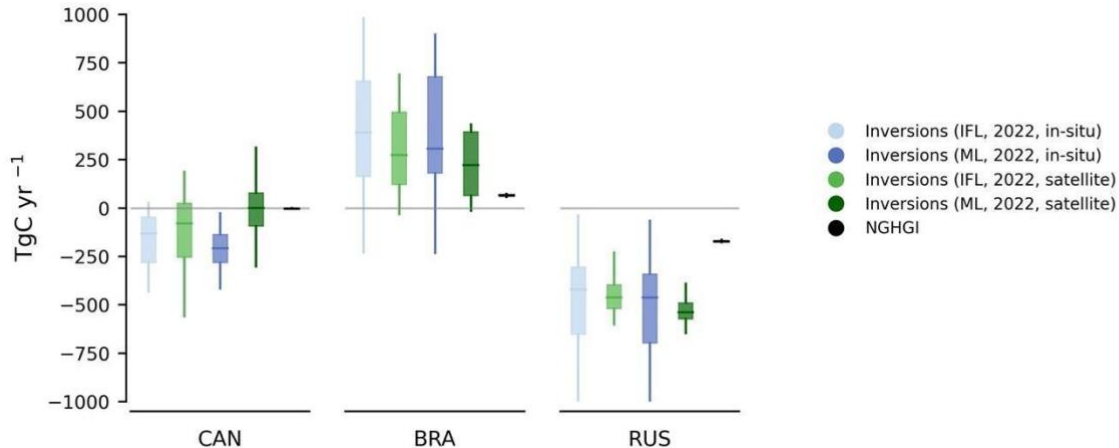
769
 770 **Figure 8.** Net CO₂ land fluxes during the period of a) 2011-2015; and b) 2016-2020 in China (CHN), United States (USA), European
 771 Union (EUR), Russia (RUS), Canada (CAN), Kazakhstan (KAZ), Mongolia (MNG), India (IND), Brazil (BRA), Democratic Republic
 772 of the Congo (COD), South Africa (ZAF), and Australia (AUS). Blue boxes denote the in-situ inversion results from Deng et al. (2022)
 773 processed from Global Carbon Budget 2020 (Friedlingstein et al., 2020). Light green boxes denote the in-situ inversion results processed in
 774 this study, while dark green boxes denote the satellite inversion results. Black boxes denote the NGHGs reported values. The white lines in

775 the boxes denote the medians of the land CO₂ fluxes. Note that the inversion results here have been adjusted by the lateral flux before the
776 comparison. Additionally, we extend the comparison with national land use change emissions from global bookkeeping models in Fig S4.
777 In this section, we compare four different estimates of land CO₂ fluxes during the period 2010-2020 (**Fig 8**), including: 1)
778 medians of in-situ inversion results from our previous study (Deng et al., 2022), 2) medians of in-situ and 3) satellite-based
779 inversion results processed in this study based on the Global Carbon Budget 2022 (Friedlingstein et al., 2022), and 4) NGHGIs.
780 This enables a comparison of the median and range of our in-situ inversion results (n=5) with those from previous study (n=6),
781 and assesses the performance differences between satellite-based (n=4) and in-situ inversion models. To ensure a fair
782 comparison and avoid anomalies in the satellite-based inversion results during 2010-2015 when some of these inversions used
783 GOSAT after 2010 and then OCO-2 after 2015, we separate the analysis into two periods: 2011-2015 and 2016-2020.
784 The variations of yearly land CO₂ fluxes span a comparable range between the current and previous in-situ inversion
785 ensembles, indicating that consistency of the inversion results, but the uncertainty within the new in-situ inversion ensemble
786 was not improved. However, examining the median values, results from the new in-situ inversion ensemble may be closer to
787 NGHGIs in most countries (such as China (CHN), United States (USA), European Union (EUR), Canada (CAN), Kazakhstan
788 (KAZ), India (IND)). This suggests that the new in-situ inversion ensemble used in this study has partially narrowed down the
789 gaps between inversion results and NGHGIs compared to the previous one. However, in Russia (RUS) and Brazil (BRA), the
790 difference between the median of in-situ inversion ensembles and NGHGIs has enlarged. For example, in RUS, median the
791 new in-situ inversion ensemble indicate a larger carbon sink than those from Deng et al. (2022), while the difference between
792 median of in-situ inversions and NGHGIs increases 51% during 2011-2015 (from 208 Tg C/yr to 314 Tg C/yr) and 49% during
793 2016-2020 (from 168 Tg C/yr to 249 Tg C/yr). Conversely, in BRA, median of the new in-situ inversion ensemble indicate a
794 larger carbon source, while the difference increases over 100% during 2011-2015 (from 200 Tg C/yr to 423 Tg C/yr) and
795 nearly 300% during 2016-2020 (from 56 Tg C/yr to 223 Tg C/yr).

796 As for the inversion ensemble used in this study, in most countries, the variations of yearly land CO₂ fluxes also span a similar
797 range between satellite-based inversion ensemble and in-situ inversion ensemble. However, in the cases of USA, RUS, CHN
798 and BRA, the spread of satellite-based inversion results are narrower than those of in-situ inversion results, indicating a better
799 consistency among available satellite-based inversion models, at least when similar satellite data are assimilated. In addition,
800 in most cases, smaller differences were found between the median of inversion results and the NGHGIs. For countries with
801 dense surface monitoring networks such as in the USA and EUR, the satellite-based inversion results show good agreement
802 in-situ inversion results. However, for countries with sparse station coverage like Kazakhstan (KAZ) and Mongolia (MNG),
803 satellite-based inversion results could provide more reliable estimates due to more extensive spatial sampling from satellites,
804 although the medians of satellite-based inversion results indicate larger carbon sinks and larger differences compared with
805 NGHGIs (than for in-situ inversion results). In USA and CAN, the difference during 2011-2015 (only GOSAT period) between
806 in-situ and satellite-based inversion ensembles is larger than that during 2016-2020 (OCO-2 period). This can be attributed to
807 the use of different satellite data during these periods and different numbers of ensemble members. Before 2015, only GOSAT

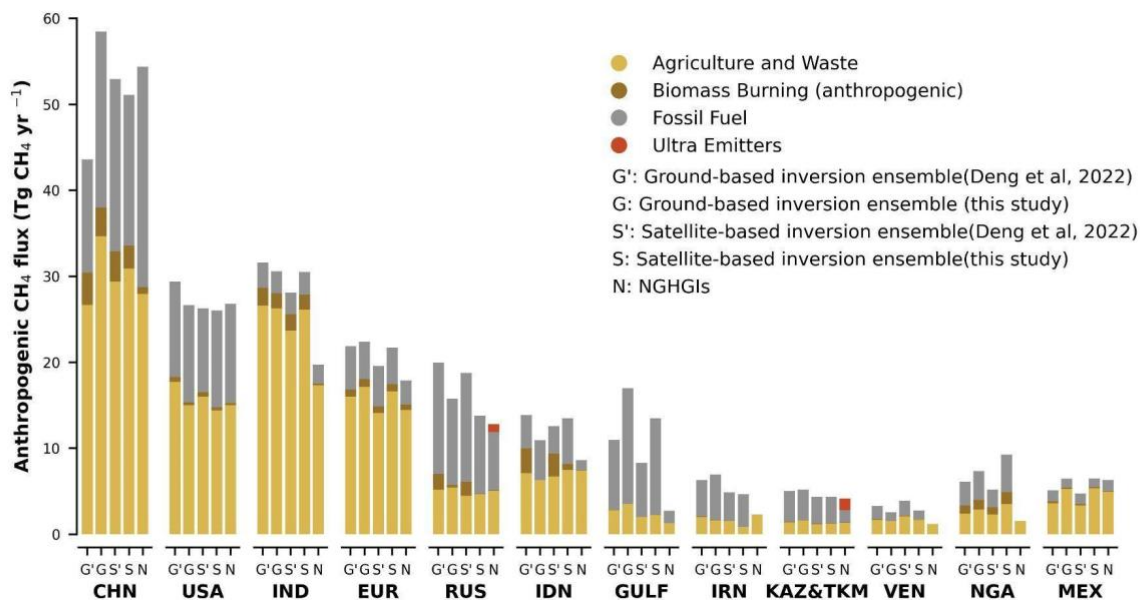
808 was available, and only 2 out of 4 systems. The inversion of OCO-2 data starting in 2014 resulted in a better alignment among
809 OCO-2 ACOS v10 inversions, indicating the in-situ and satellite evaluations were similar (Byrne et al., 2023).

810 6.2 Adjustment of the national managed land masks to separate the net land CO₂ flux estimates



811
812 **Figure 9. Net CO₂ land fluxes during the period of 2015-2020 in Canada (CAN), Brazil (BRA), and Russia (RUS).** ‘IFL’ stands for
813 using the intact forest landscape data as a mask for non-managed land to extract land CO₂ flux from managed land and ‘ML’ indicates the
814 adjusted mask used by Grassi et al. (2023) to extract land CO₂ flux from managed land. The ‘in-situ’ stands for inversion results using in-
815 situ observations, and ‘satellite’ represents inversions using satellite observations. Note that the inversion results here have been adjusted by
816 the lateral flux before the comparison.

817 Following the method proposed by Grassi et al. (2023), we updated in this study the managed land mask for Canada (CAN)
818 and Brazil (BRA) by using maps of managed land derived from NGHGI, and for Russia (RUS) by adjusting tree-cover
819 threshold in the tree cover map from Hansen et al. (2013) to match the average area of managed land per Oblast (province)
820 that is used for the NGHGIs. Thus, the new mask is now more consistent with the definition of managed land in the NGHGIs
821 for these three countries, so that can further analyze the impacts of different definitions of managed land masks to separate the
822 managed land CO₂ fluxes in inversions (**Fig 9**). Generally, in Russia (RUS) and Canada (CAN), the managed land CO₂ fluxes
823 extracted from the new mask are closer to NGHGIs than those separated by the previous mask used by Deng et al. 2022. In
824 addition, in Brazil (BRA), adjusting the national managed land mask resulted in greater land carbon emissions, increasing the
825 gap with NGHGIs. However, the improvement of the managed land mask in this study is still not able to explain all the existing
826 discrepancy between inversion estimates and NGHGIs, in which the sources and reasons for these differences and uncertainties
827 still need further analysis. We also observe in **Fig. 9** that the impact of our new managed land mask compared to the previous
828 one, is qualitatively similar whether it is applied to in-situ inversions or satellite inversions gridded flux fields.



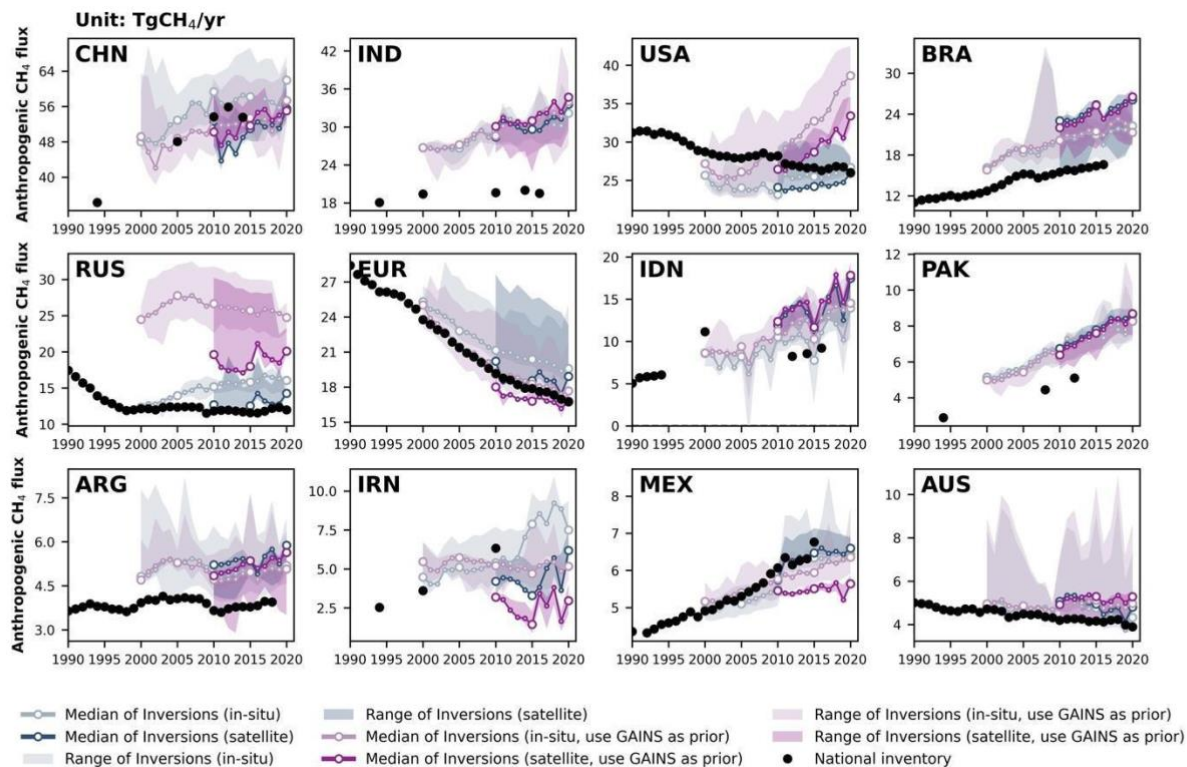
830

831 **Figure 10. Annual average of anthropogenic CH₄ emissions from in-situ (G) and satellite (S) inversions and national greenhouse gas**
 832 **inventories (N) during the period of 2010-2020. G' and S' denote the anthropogenic CH₄ flux from the in-situ and satellite inversion**
 833 **ensembles in the previous study (Deng et al., 2022) respectively, while G and S denote the fluxes from the in-situ and satellite inversion**
 834 **ensembles used in this study. N denotes the estimates from NGHGs. Grey, yellow, and brown bars represent the CH₄ fluxes from the sectors**
 835 **of fossil fuel combustion, agriculture and waste, and biomass burning respectively. On top of NGHGI emissions, emissions from ultra-**
 836 **emitters (red) are added to NGHGI estimates (diagnosed from S5P-TROPOMI measurements for the period 2019–2020; Lauvaux et al.,**
 837 **2022).**

838 In our previous study, we found that satellite inversion models appear to have a better agreement with NGHGs than in-situ
 839 stations based inversion models, and on the other hand, that differences between inversion models and NGHGs in large oil-
 840 and gas-producing countries suggest an underestimation of national reports, possibly due to the omission of ultra-emitting
 841 sources by NGHGs. With the new inversion ensemble in this study, we confirm those results (**Fig 10**). In countries such as
 842 China (CHN), India (IND), and Russia (RUS), the updated inversion model set provides estimates that are closer to NGHGs,
 843 but differences still exist, and the reasons for these differences are not the same. For example, differences in anthropogenic
 844 methane emissions in IND are mainly due to differences in agricultural and waste methane flux with the new inversion
 845 ensemble used in this study. In RUS, the updated inversion ensemble shows lower fossil fuel emissions, reducing the
 846 differences with NGHGs for this sector, but higher agricultural and waste emissions than in Deng et al. (2022). Nevertheless,
 847 the updated fossil fuel emission flux is still higher than the NGHGs estimate for RUS. The remaining differences may be
 848 attributed to ultra-emitting sources or underestimated emission factors for some components of the oil and gas extraction and
 849 distribution industry in RUS. Conversely, in GULF (GULF = Saudi Arabia + Iraq + Kuwait + Oman + United Arab Emirates

850 + Bahrain + Qatar), the new inversion model ensemble consistently reflects higher fossil fuel emission fluxes than NGHGs
 851 like in our previous study, and expands the difference in estimates of artificial methane flux between inversion models and
 852 NGHGs, possibly indicating more methane leakage.

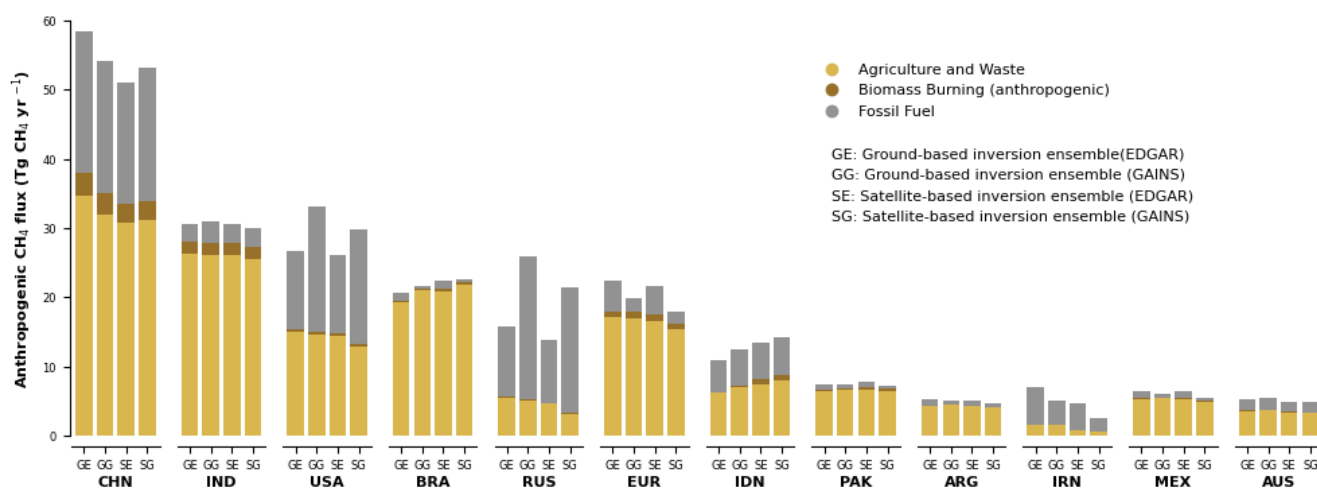
853 6.4 Influence of the prior used in CH₄ inversions



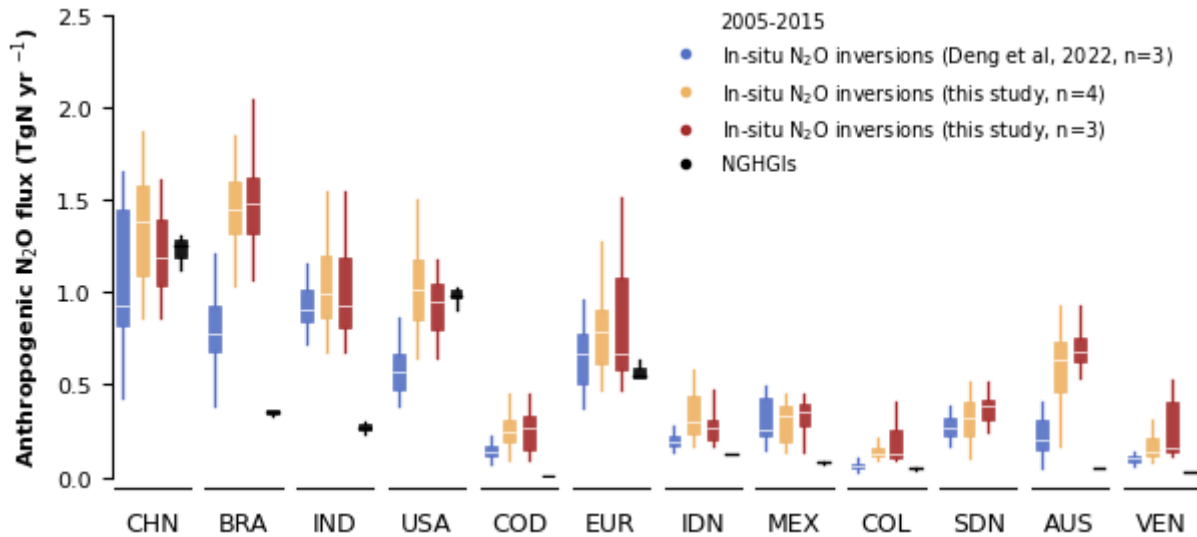
854
 855 **Figure 11. Total anthropogenic CH₄ fluxes for the 12 top emitters: China (CHN), India (IND), United States (USA), Brazil (BRA),**
 856 **Russia (RUS), European Union (EUR), Indonesia (IDN), Pakistan (PAK), Argentina (ARG), Iran (IRN), Mexico (MEX), and**
 857 **Australia (AUS).** The black dots denote the reported values from NGHGs. The light blue lines/areas denote the median and maximum-
 858 minimum ranges of in-situ CH₄ inversions based on EDGARv6.0 as the prior and the dark blue ones of satellite inversions, respectively.
 859 The light purple lines/areas denote the median and maximum-minimum ranges of in-situ CH₄ inversions based on GAINS (Höglund-Isaksson
 860 et al., 2020) as the prior and the dark purple ones of satellite inversions, respectively.

861
 862 The use of different priors can also influence the inversion results of the data. **Fig 11** presents the sets of inversion results using
 863 EDGAR (blue) and GAINS (purple) as priors. In most countries, the median values of the two inversion result sets are similar.
 864 However, in countries such as Russia (RUS), United States (USA), Iran (IRN), Mexico (MEX), significant differences are
 865 observed between the two inversion result sets, which may primarily stem from the differences in the inversion results for
 866 fossil CH₄ emissions (**Fig 12**). In RUS and USA, the inversion results using GAINS as priors are consistently higher than those

867 using EDGAR as priors. In RUS, the satellite inversion results using GAINS as priors are higher by 45% during 2010-2020,
 868 and the ground-based inversion results are higher by 75% during 2000-2020. In the case of the USA, the inversion results
 869 using GAINS as priors exhibit a completely different trend compared to the ones obtained using NGHGs and EDGAR as
 870 priors. The inversion results using GAINS as priors, both from satellite and ground-based measurements, show a rapid growth
 871 trend by increasing 24% from 2010 to 2020. In IRN and MEX, the inversion results using GAINS as priors are lower than
 872 those using EDGAR as priors. For IRN, the differences between satellite inversion results using different priors are not
 873 significant, and the trends are similar. However, the ground-based inversion results are very close between 2000-2013, but
 874 after 2013, a steep increase is observed in the ground-based inversion results using GAINS as priors. On the other hand, in
 875 MEX, the ground-based inversion results are similar, but the satellite inversion results using GAINS as priors are relatively
 876 lower by 14% averagely. Such discrepancies may arise from differences in inventory methodologies and the resulting
 877 estimations. As shown in Supplementary Figure S1 in Tibrewal et al. (2024), similar discrepancies were found between the
 878 two inventories in these countries, which reports a higher estimation from GAINS in RUS and USA compared to EDGAR
 879 during 2011-2020, and a lower estimation in IRN. As noted in Tibrewal et al. (2024), EDGAR is based on various versions of
 880 National Inventory Reports (NIR) that utilize different combinations of emission factors from the IPCC, while GAINS employs
 881 an independent estimation approach. This highlights the critical role of prior data selection in determining the accuracy of CH₄
 882 emission estimates.



883
 884 Fig 12. Annual average of anthropogenic CH₄ emissions from in-situ and satellite inversions based on two different priors
 885 during the period of 2010-2020. GE and SE denote the anthropogenic CH₄ flux from the in-situ and satellite inversion
 886 ensembles based on EDGARv6.0 as the prior, while GG and SG represent the in-situ and satellite CH₄ inversions based on
 887 GAINS as the prior.



889
890 **Figure 13. Anthropogenic N₂O fluxes during the period of 2005-2015 in China (CHN), Brazil (BRA), India (IND), United States**
891 **(USA), Democratic Republic of the Congo (COD), European Union (EUR), Indonesia (IDN), Mexico (MEX), Colombia (COL), SDN**
892 **(Sudan), Australia (AUS), and Venezuela (VEN).** Blue boxes denote the in-situ inversion results from Deng et al. 2022 processed from
893 Global Carbon Budget 2020 (Friedlingstein et al., 2020). Dark yellow boxes denote the inversion results processed in this study. Black boxes
894 denote the NGHGIs reported values.

895
896 The updated N₂O inversion results show systematically higher anthropogenic emissions than the previous N₂O inversion results
897 (Deng et al, 2022), resulting in larger discrepancies between N₂O inversion results and NGHGIs in most countries in Fig 13,
898 Countries such as Brazil (BRA), Democratic Republic of the Congo (COD), Indonesia (IDN), Colombia (COL), Sudan (SDN),
899 Australia (AUS), and Venezuela (VEN) exhibit significant differences. These discrepancies may be attributed to the use of
900 lower IPCC default emission factors in the national inventories of these tropical countries, leading to lower NGHGI results.
901 The IPCC default emission factors are derived from measurements primarily conducted in temperate regions of the Northern
902 Hemisphere (e.g., Europe and the United States (USA)), which explains the better alignment of inversion results with
903 inventories in those regions. Notably, , in the case of the USA, the median of the updated N₂O inversion results is very close
904 to NGHGIs. The median of the N₂O inversion results from Deng et al. (2022) was 42% lower than the NGHGIs between 2005
905 and 2015, whereas the median of the updated inversion models is only 4% lower. This demonstrates improved consistency in
906 the updated inversion system results for the USA. Additionally, in countries such as India (IND), IDN, COL, COD, Sudan
907 (SDN), and VEN, our N₂O inversion results have a larger distribution compared to the previous study, indicating that the new
908 N₂O inversion ensemble (n=4) has less consistency in these countries compared to the previous ensemble (n=3).

909 **Conclusions**

910 This study reconciles the gap between atmospheric inversions and UNFCCC NGHGs for each of the three greenhouse gases,
911 based on the post-processing framework we proposed in our previous study (Deng et al., 2022). We update inversion results
912 and NGHGs datasets to present the most-up-to-date discrepancies between these two estimates. For CO₂, we updated the
913 inversion results up to 2021, added a new inversion ensemble including inversions based on satellite observations, and applied
914 a new mask of national managed land based on NGHGI reports in Russia, Brazil and Canada. For CH₄, we compared NGHGs
915 and CH₄ inversion results up to 2020 by splitting the anthropogenic fluxes from inversions by aggregating prior estimates from
916 each sector or by removing fluxes of natural processes and discussed the uncertainties by using different priors in CH₄
917 inversions. For N₂O, we updated the inversion results up to 2019 and included the MIROC4-ACTM N₂O inversion, also
918 separated the fluxes from managed land by using the same method on CO₂.

919 In the case of CO₂, we updated the managed land mask for Canada, Brazil, and Russia based on maps derived from NGHGs
920 and adjusted tree-cover thresholds. The analysis of different managed land mask definitions shows that the new mask, which
921 is more consistent with the definition of managed land in the NGHGs for these countries, improves the agreement between
922 managed land CO₂ fluxes and NGHGs in Russia and Canada. However, in Brazil, the new mask increases the gap between
923 the estimated land carbon emissions and NGHGs. Further analysis is needed to understand the sources and reasons for
924 discrepancies and uncertainties between inversion estimates and NGHGs. Thus, we still recommend that countries should
925 report their managed land in a spatially explicit manner to enable a better evaluation of national emission reports using
926 inversions (and other observation-based approaches), and countries should also follow the recommendations of the IPCC 2006
927 Guidelines encouraging countries to use atmospheric data as an independent check on their national reports (IPCC 2006, 2019).
928 Three additional satellite-based inversion results have been introduced for comparison with the in-situ inversion results and
929 NGHGs. In some countries, the satellite-based inversions demonstrate better consistency with NGHGs compared to the in-
930 situ inversion models.

931 For CH₄, despite the large spread of inversions, both in-situ and GOSAT inversions show systematic differences with NGHGs.
932 We also found that Kazakhstan and Turkmenistan in Central Asia and the Gulf countries in the Middle East, characterized by
933 oil- and gas-producing industries, report much less CH₄ emissions than atmospheric inversions estimates. While in this region,
934 there are few ground stations, and inversions depend on their prior fluxes, the fact that GOSAT and in-situ based inversions
935 point to NGHGI emissions being underestimated suggests areas for future research to constrain the emissions of these
936 countries. We recommend here to develop regional campaigns (such as those performed in Alvarez et al. (2018)), to refine
937 emission factors, and to track regional oil, gas and coal basins emissions and ultra-emitter site-level emissions using new tools
938 (such as moderate and high-resolution satellite imagery).

939 For N₂O, the prevalence of large tropical natural sources, being outside the responsibility of countries if they are located on
940 unmanaged lands, has been overlooked before. For example, nearly half of the forests in Brazil are unmanaged according to
941 its national inventory report. We did not solve this problem, but highlighted it and proposed a new method to remove natural

942 emissions from inversion total emissions. As many non-Annex I countries, which will have to produce inventories for the
943 global stocktake are tropical countries with a very active nitrogen cycle and large natural N₂O emissions, a decoupling will
944 exist between targeted emissions reductions and the observed growth rate of N₂O: it may hamper the eventual effectiveness of
945 mitigation policies, that are directly reflected in the UNFCCC NGHGs reports, especially for this greenhouse gas. It is fair to
946 say that the uncertainty from the spread of different inversions is large enough that inversions cannot ‘falsify’ N₂O NGHGs
947 in most instances. Nevertheless, for CH₄ in countries around the Persian Gulf and Central Asia, and to some extent in Russia,
948 and for N₂O in tropical countries, Mexico and Australia, we found that NGHGs emissions are significantly lower than
949 inversions, which suggests that activity data or emission factors may need to be re-evaluated. Despite their large spread,
950 inversions have the advantage of providing fluxes that are consistent with the accurately observed growth rates of each
951 greenhouse gas in the atmosphere. The uncertainty of inversions is mainly a systematic bias due to internal settings or to the
952 choice of a transport model. It does not mean that inversions cannot be used for monitoring interannual variability and trends
953 of fluxes, in response to mitigation efforts, since most of their bias should have a small temporal component.

954 The study of global inversions at the country scale rather than at the traditional subcontinent scale (e.g. the “Transcom3
955 regions” of Gurney et al. (2002)) obviously pushes inversions close to the limit of their domain of validity, even in the case of
956 large countries. The densification of observation networks and systems, especially from space, increases the observational
957 information available at all spatial scales and gradually makes it possible to study smaller countries and reduce uncertainties
958 of inversion results. This densification must be accompanied by a corresponding increase in the horizontal resolution of
959 inversion systems (both the transport model and the control vector to be optimized). Note that the spatial resolution of most
960 inverse models such as those contributing to the global carbon/methane/nitrous oxide budget is larger than 1 degree (see Table
961 A4 in Friedlingstein et al. (2022), Table S6 in Saunio et al. (2020), and Table 1 in Tian et al. (2023)). They will likely soon
962 have to go below one degree on a global scale to remain competitive for this type of study, despite the high computational
963 challenge posed by the atmospheric inversion of long-lived tracers.

964 **Data availability**

965 Processed GHG (CO₂, CH₄, and N₂O) data from inverse models and UNFCCC NGHGs are available at
966 <https://doi.org/10.5281/zenodo.13887128> (Deng et al., 2024).

967 This dataset contains 5 data files:

- 968 - The file *Inversions_CO2_v2022.csv* includes the NEE CO₂ flux from managed lands for the nine CO₂ inverse
969 models. It includes 8 fields: years (from 1960 to 2021), country, value (unit: Tg C/yr), sector ("land": without the
970 adjustment of lateral C flux; "land_cor": with later C flux adjustment), source, gas, observation ("in-situ": in-situ-
971 based; "satellite": satellite-based), version ("CO₂_ML_v2022" only).
- 972 - The file *Inversions_CH4_v2022.csv* includes CH₄ flux from anthropogenic sources for the six CH₄ inverse models.
973 It includes 8 fields: years (from 2000 to 2020), country, value (unit: Tg CH₄/yr), sector ("agr": agriculture and

waste; "fos": fossil fuel; "ant": anthropogenic=agrw+fos), source, gas, observation ("in-situ": in-situ-based; "satellite": satellite-based), version ("CH4_2022_V1": use EDGAR as priors; "CH4_2022_V2": use GAINS as priors).

- The file *Inversions_N2O_v2022.csv* includes the anthropogenic N2O flux from managed lands for the four N2O inversion models. It includes 8 fields: years (from 1995 to 2020), country, value (unit: TgN2O/yr), sector ("ant" only, for anthropogenic), source, gas, observation ("in-situ" only, for in-situ-based), version ("N2O_ML_v2022" only).
- The file *lateral_CO2_v2022.csv* includes the national lateral C flux from river and trade.
- The file *NGHGs_v2022.csv* includes the national inventory data collected from UNFCCC NGHGs (unit: Gg/yr)

Author contribution

PC, FC, MS, RLT, and ZD designed and coordinated the study. PC, MS, RLT, and FC designed the framework of atmosphere inversion data processing. ZD, PC, LH, MS, RLT, and FC performed the post-processing and analysis and wrote the paper. ZD, LH, and TW compiled the national greenhouse gas inventories. MS, RLT, HT, and FC gathered the global atmosphere inversion datasets of CO₂, CH₄, and N₂O. GG contributed the managed land mask of Brazil and Canada. FC processed the atmosphere inversion data with masks of managed lands and country boundaries. AT, SM, RJ, YN, BZ, JT, DB and AS contribute the unpublished CH₄ inversion data. All authors contributed to the full text.

Competing interests

At least one of the (co-)authors is a member of the editorial board of Earth System Science Data.

Acknowledgements

The authors are very grateful to the atmosphere inversion model developers Chris Wilson, Christian Rödenbeck, Kelley Wells, Liesbeth Florentie, Naveen Chandra, Peter Bergamaschi, Prabir Patra, and Yi Yin for the availability of their global CO₂, CH₄, and N₂O inversion data and acknowledge many other data providers (measurements, models, inventories, atmospheric inversions, hybrid products, etc.) that are directly or indirectly used in this synthesis. The PyVAR-CAMS N₂O modelling results were funded through the Copernicus Atmospheric Monitoring Service, implemented by ECMWF on behalf of the European Commission and were generated using computing resources from LSCE. Rona Thompson would also like to acknowledge the support of Frederic Chevallier in providing the PyVAR-CAMS N₂O inversion results.

References

Aragão, L. E. O. C., Anderson, L. O., Fonseca, M. G., Rosan, T. M., Vedovato, L. B., Wagner, F. H., Silva, C. V. J., Silva Junior, C. H. L.,

1001 Arai, E., Aguiar, A. P., Barlow, J., Berenguer, E., Deeter, M. N., Domingues, L. G., Gatti, L., Gloor, M., Malhi, Y., Marengo, J. A.,
1002 Miller, J. B., Phillips, O. L., and Saatchi, S.: 21st Century drought-related fires counteract the decline of Amazon deforestation
1003 carbon emissions, *Nat. Commun.*, 9, 536, 2018.

1004 Berchet, A., Sollum, E., Thompson, R. L., Pison, I., Thanwerdas, J., Broquet, G., Chevallier, F., Aalto, T., Berchet, A., Bergamaschi, P.,
1005 Brunner, D., Engelen, R., Fortems-Cheiney, A., Gerbig, C., Groot Zwaafink, C. D., Haussaire, J.-M., Henne, S., Houweling, S.,
1006 Karstens, U., Kutsch, W. L., Lujikx, I. T., Monteil, G., Palmer, P. I., van Peet, J. C. A., Peters, W., Peylin, P., Potier, E., Rödenbeck,
1007 C., Saunio, M., Scholze, M., Tsuruta, A., and Zhao, Y.: The Community Inversion Framework v1.0: a unified system for
1008 atmospheric inversion studies, *Geoscientific Model Development*, 14, 5331–5354, 2021.

1009 Byrne, B., Liu, J., Lee, M., Yin, Y., Bowman, K. W., Miyazaki, K., Norton, A. J., Joiner, J., Pollard, D. F., Griffith, D. W. T., Velazco, V.
1010 A., N. M. Deutscher, Jones, N. B., and Paton-Walsh, C.: The carbon cycle of southeast Australia during 2019–2020: Drought, fires,
1011 and subsequent recovery, *AGU Advances*, 2, <https://doi.org/10.1029/2021av000469>, 2021.

1012 Byrne, B., Baker, D. F., Basu, S., Bertolacci, M., Bowman, K. W., Carroll, D., Chatterjee, A., Chevallier, F., Ciais, P., Cressie, N., Crisp,
1013 D., Crowell, S., Deng, F., Deng, Z., Deutscher, Nicholas M., Dubey, M. K., Feng, S., García, O. E., Griffith, D. W. T., Herkommer,
1014 B., Hu, L., Jacobson, A. R., Janardanan, R., Jeong, S., Johnson, M. S., Jones, D. B. A., Kivi, R., Liu, J., Liu, Z., Maksyutov, S.,
1015 Miller, J. B., Miller, S. M., Morino, I., Notholt, J., Oda, T., O'Dell, C. W., Oh, Y.-S., Ohyama, H., Patra, P. K., Peiro, H., Petri, C.,
1016 Philip, S., Pollard, D. F., Poulter, B., Remaud, M., Schuh, A., Sha, M. K., Shiomi, K., Strong, K., Sweeney, C., Té, Y., Tian, H.,
1017 Velazco, V. A., Vrekoussis, M., Warneke, T., Worden, J. R., Wunch, D., Yao, Y., Yun, J., Zammit-Mangion, A., and Zeng, N.:
1018 National CO₂ budgets (2015–2020) inferred from atmospheric CO₂ observations in support of the global stocktake, *Earth System
1019 Science Data*, 15, 963–1004, 2023.

1020 Chandra, N., Patra, P. K., Bisht, J. S. H., Ito, A., Umezawa, T., Saigusa, N., Morimoto, S., Aoki, S., Janssens-Maenhout, G., Fujita, R.,
1021 Takigawa, M., Watanabe, S., Saitoh, N., and Canadell, J. G.: Emissions from the Oil and Gas Sectors, Coal Mining and Ruminant
1022 Farming Drive Methane Growth over the Past Three Decades, *Journal of the Meteorological Society of Japan. Ser. II*, 99, 309–337,
1023 2021.

1024 Chang, J., Ciais, P., Gasser, T., Smith, P., Herrero, M., Havlík, P., Obersteiner, M., Guenet, B., Goll, D. S., Li, W., Naipal, V., Peng, S.,
1025 Qiu, C., Tian, H., Viovy, N., Yue, C., and Zhu, D.: Climate warming from managed grasslands cancels the cooling effect of carbon
1026 sinks in sparsely grazed and natural grasslands, *Nat. Commun.*, 12, 118, 2021.

1027 Chevallier, F.: Fluxes of carbon dioxide from managed ecosystems estimated by national inventories compared to atmospheric inverse
1028 modeling, *Geophys. Res. Lett.*, 48, <https://doi.org/10.1029/2021gl093565>, 2021.

1029 Chevallier, F., Fisher, M., Peylin, P., Serrar, S., Bousquet, P., Bréon, F.-M., Chédin, A., and Ciais, P.: Inferring CO₂ sources and sinks
1030 from satellite observations: Method and application to TOVS data, *J. Geophys. Res.*, 110, <https://doi.org/10.1029/2005jd006390>,
1031 2005.

1032 Ciais, P., Yao, Y., Gasser, T., Baccini, A., Wang, Y., Lauerwald, R., Peng, S., Bastos, A., Li, W., Raymond, P. A., Canadell, J. G., Peters,
1033 G. P., Andres, R. J., Chang, J., Yue, C., Dolman, A. J., Haverd, V., Hartmann, J., Laruelle, G., Konings, A. G., King, A. W., Liu, Y.,
1034 Luysaert, S., Maignan, F., Patra, P. K., Peregon, A., Regnier, P., Pongratz, J., Poulter, B., Shvidenko, A., Valentini, R., Wang, R.,
1035 Broquet, G., Yin, Y., Zscheischler, J., Guenet, B., Goll, D. S., Ballantyne, A.-P., Yang, H., Qiu, C., and Zhu, D.: Empirical estimates
1036 of regional carbon budgets imply reduced global soil heterotrophic respiration, *Natl Sci Rev*, 8, nwaal45, 2021.

1037 Cui, X., Zhou, F., Ciais, P., Davidson, E. A., Tubiello, F. N., Niu, X., Ju, X., Canadell, J. G., Bouwman, A. F., Jackson, R. B., Mueller, N.
1038 D., Zheng, X., Kanter, D. R., Tian, H., Adalbieke, W., Bo, Y., Wang, Q., Zhan, X., and Zhu, D.: Global mapping of crop-specific
1039 emission factors highlights hotspots of nitrous oxide mitigation, *Nat Food*, 2, 886–893, 2021.

1040 Deng, Z., Ciais, P., Tzompa-Sosa, Z. A., Saunio, M., Qiu, C., Tan, C., Sun, T., Ke, P., Cui, Y., Tanaka, K., Lin, X., Thompson, R. L.,
1041 Tian, H., Yao, Y., Huang, Y., Lauerwald, R., Jain, A. K., Xu, X., Bastos, A., Sitch, S., Palmer, P. I., Lauvaux, T., d’Aspremont, A.,
1042 Giron, C., Benoit, A., Poulter, B., Chang, J., Petrescu, A. M. R., Davis, S. J., Liu, Z., Grassi, G., Albergel, C., Tubiello, F. N.,
1043 Perugini, L., Peters, W., and Chevallier, F.: Comparing national greenhouse gas budgets reported in UNFCCC inventories against
1044 atmospheric inversions, *Earth Syst. Sci. Data*, 14, 1639–1675, 2022.

1045 Deng, Z., Ciais, P., Hu, L., Wang, T., Martinez, A., Saunio, M., Thompson, R., and Chevallier, F.: Global greenhouse gas reconciliation
1046 2022, 2024. <https://doi.org/10.5281/zenodo.13887128>

1047 FAO: Trade, FAOSTAT, 2024. available at: <https://www.fao.org/faostat/en/#data>. FAO, Rome, Italy.

1048 Feng, L., Palmer, P. I., Parker, R. J., N. M. Deutscher, Feist, D. G., Kivi, R., Morino, I., and Sussmann, R.: Estimates of European uptake
1049 of CO₂ inferred from GOSAT XCO₂ retrievals: sensitivity to measurement bias inside and outside Europe, *Atmos. Chem. Phys.*, 16,
1050 1289–1302, 2016.

1051 Flammini, A., Adzmir, H., Karl, K., and Tubiello, F. N.: Quantifying greenhouse gas emissions from wood fuel use by households, *Earth*
1052 *Syst. Sci. Data*, 15, 2179–2187, <https://doi.org/10.5194/essd-15-2179-2023>, 2023.

1053 Friedlingstein, P., O’Sullivan, M., Jones, M. W., Andrew, R. M., Hauck, J., Olsen, A., Peters, G. P., Peters, W., Pongratz, J., Sitch, S., Le
1054 Quéré, C., Canadell, J. G., Ciais, P., Jackson, R. B., Alin, S., Aragão, L. E. O. C., Arneeth, A., Arora, V., Bates, N. R., Becker, M.,
1055 Benoit-Cattin, A., Bittig, H. C., Bopp, L., Bultan, S., Chandra, N., Chevallier, F., Chini, L. P., Evans, W., Florentie, L., Forster, P.
1056 M., Gasser, T., Gehlen, M., Gilfillan, D., Gkritzalis, T., Gregor, L., Gruber, N., Harris, I., Hartung, K., Haverd, V., Houghton, R. A.,

1057 Ilyina, T., Jain, A. K., Joetzjer, E., Kadono, K., Kato, E., Kitidis, V., Korsbakken, J. I., Landschützer, P., Lefèvre, N., Lenton, A.,
1058 Lienert, S., Liu, Z., Lombardozzi, D., Marland, G., Metzl, N., Munro, D. R., Nabel, J. E. M. S., Nakaoka, S.-I., Niwa, Y., O'Brien,
1059 K., Ono, T., Palmer, P. I., Pierrot, D., Poulter, B., Resplandy, L., Robertson, E., Rödenbeck, C., Schwinger, J., Séférian, R., Skjelvan,
1060 I., Smith, A. J. P., Sutton, A. J., Tanhua, T., Tans, P. P., Tian, H., Tilbrook, B., van der Werf, G., Vuichard, N., Walker, A. P.,
1061 Wanninkhof, R., Watson, A. J., Willis, D., Wiltshire, A. J., Yuan, W., Yue, X., and Zaehle, S.: Global carbon budget 2020, *Earth*
1062 *Syst. Sci. Data*, 12, 3269–3340, 2020.

1063 Friedlingstein, P., O'Sullivan, M., Jones, M. W., Andrew, R. M., Gregor, L., Hauck, J., Le Quéré, C., Luijkx, I. T., Olsen, A., Peters, G. P.,
1064 Peters, W., Pongratz, J., Schwingshackl, C., Sitch, S., Canadell, J. G., Ciais, P., Jackson, R. B., Alin, S. R., Alkama, R., Arneeth, A.,
1065 Arora, V. K., Bates, N. R., Becker, M., Bellouin, N., Bittig, H. C., Bopp, L., Chevallier, F., Chini, L. P., Cronin, M., Evans, W., Falk,
1066 S., Feely, R. A., Gasser, T., Gehlen, M., Gkritzalis, T., Gloege, L., Grassi, G., Gruber, N., Gürses, Ö., Harris, I., Hefner, M.,
1067 Houghton, R. A., Hurtt, G. C., Iida, Y., Ilyina, T., Jain, A. K., Jersild, A., Kadono, K., Kato, E., Kennedy, D., Klein Goldewijk, K.,
1068 Knauer, J., Korsbakken, J. I., Landschützer, P., Lefèvre, N., Lindsay, K., Liu, J., Liu, Z., Marland, G., Mayot, N., McGrath, M. J.,
1069 Metzl, N., Monacci, N. M., Munro, D. R., Nakaoka, S.-I., Niwa, Y., O'Brien, K., Ono, T., Palmer, P. I., Pan, N., Pierrot, D., Pöcöck,
1070 K., Poulter, B., Resplandy, L., Robertson, E., Rödenbeck, C., Rodriguez, C., Rosan, T. M., Schwinger, J., Séférian, R., Shutler, J. D.,
1071 Skjelvan, I., Steinhoff, T., Sun, Q., Sutton, A. J., Sweeney, C., Takao, S., Tanhua, T., Tans, P. P., Tian, X., Tian, H., Tilbrook, B.,
1072 Tsujino, H., Tubiello, F., van der Werf, G. R., Walker, A. P., Wanninkhof, R., Whitehead, C., Willstrand Wranne, A., et al.: Global
1073 Carbon Budget 2022, *Earth System Science Data*, 14, 4811–4900, 2022.

1074 Gatti, L. V., Basso, L. S., Miller, J. B., Gloor, M., Gatti Domingues, L., Cassol, H. L. G., Tejada, G., Aragão, L. E. O. C., Nobre, C.,
1075 Peters, W., Marani, L., Arai, E., Sanches, A. H., Corrêa, S. M., Anderson, L., Von Randow, C., Correia, C. S. C., Crispim, S. P., and
1076 Neves, R. A. L.: Amazonia as a carbon source linked to deforestation and climate change, *Nature*, 595, 388–393, 2021.

1077 Gatti, L. V., Cunha, C. L., Marani, L., Cassol, H. L. G., Messias, C. G., Arai, E., Denning, A. S., Soler, L. S., Almeida, C., Setzer, A.,
1078 Domingues, L. G., Basso, L. S., Miller, J. B., Gloor, M., Correia, C. S. C., Tejada, G., Neves, R. A. L., Rajao, R., Nunes, F., Filho, B.
1079 S. S., Schmitt, J., Nobre, C., Corrêa, S. M., Sanches, A. H., Aragão, L. E. O. C., Anderson, L., Von Randow, C., Crispim, S. P.,
1080 Silva, F. M., and Machado, G. B. M.: Increased Amazon carbon emissions mainly from decline in law enforcement, *Nature*, 621,
1081 318–323, 2023.

1082 Grassi, G., Stehfest, E., Rogelj, J., van Vuuren, D., Cescatti, A., House, J., Nabuurs, G.-J., Rossi, S., Alkama, R., Viñas, R. A., Calvin, K.,
1083 Ceccherini, G., Federici, S., Fujimori, S., Gusti, M., Hasegawa, T., Havlik, P., Humpenöder, F., Korosuo, A., Perugini, L., Tubiello,
1084 F. N., and Popp, A.: Critical adjustment of land mitigation pathways for assessing countries' climate progress, *Nat. Clim. Chang.*, 11,

1085 425–434, 2021.

1086 Grassi, G., Schwingshackl, C., Gasser, T., Houghton, R. A., Sitch, S., Canadell, J. G., Cescatti, A., Ciais, P., Federici, S., Friedlingstein, P.,
1087 Kurz, W. A., Sanz Sanchez, M. J., Abad Viñas, R., Alkama, R., Bultan, S., Ceccherini, G., Falk, S., Kato, E., Kennedy, D., Knauer,
1088 J., Korosuo, A., Melo, J., McGrath, M. J., Nabel, J. E. M. S., Poulter, B., Romanovskaya, A. A., Rossi, S., Tian, H., Walker, A. P.,
1089 Yuan, W., Yue, X., and Pongratz, J.: Harmonising the land-use flux estimates of global models and national inventories for 2000–
1090 2020, *Earth System Science Data*, 15, 1093–1114, 2023.

1091 Hartmann, J., Jansen, N., Dürr, H. H., Kempe, S., and Köhler, P.: Global CO₂-consumption by chemical weathering: What is the
1092 contribution of highly active weathering regions?, *Glob. Planet. Change*, 69, 185–194, 2009.

1093 Höglund-Isaksson, L., Gómez-Sanabria, A., Klimont, Z., Rafaj, P., and Schöpp, W.: Technical potentials and costs for reducing global
1094 anthropogenic methane emissions in the 2050 timeframe –results from the GAINS model, *Environ. Res. Commun.*, 2, 025004, 2020.

1095 IPCC: Revised 1996 IPCC Guidelines for National Greenhouse Inventories, IPCC/OECD/IEA, Paris, France, 1997.

1096 IPCC: 2006 IPCC guidelines for National Greenhouse Gas Inventories, IGES, 2006.

1097 IPCC: 2019 Refinement to the 2006 IPCC Guidelines for National Greenhouse Gas Inventories, edited by: Buendia, E., Tanabe, K.,
1098 Kranjc, A., Baasansuren, J., Fukuda, M., Ngarize, S., Osako, A., Pyrozhenko, Y., Shermanau, P., and Federici, S., Intergovernmental
1099 Panel on Climate Change (IPCC), Switzerland, 2019.

1100 IPCC: Climate Change 2023: Synthesis Report, IPCC, Geneva, Switzerland, 2023.

1101 Janardanan, R., Maksyutov, S., Wang, F., Nayagam, L., Sahu, S., Mangaraj, P., Saunio, M., Lan, X., and Matsunaga, T.: Country-level
1102 methane emissions and their sectoral trends during 2009–2020 estimated by high-resolution inversion of GOSAT and surface
1103 observations, *Environmental Research Letters*, 19, 10.1088/1748-9326/ad2436, 2024

1104 Janssens-Maenhout, G., Crippa, M., Guizzardi, D., Muntean, M., Schaaf, E., Dentener, F., Bergamaschi, P., Pagliari, V., Olivier, J. G. J.,
1105 Peters, J. A. H. W., van Aardenne, J. A., Monni, S., Doering, U., Petrescu, A. M. R., Solazzo, E., and Oreggioni, G. D.: EDGAR
1106 v4.3.2 Global Atlas of the three major greenhouse gas emissions for the period 1970–2012, *Earth Syst. Sci. Data*, 11, 959–1002,
1107 2019.

1108 Jin, Z., Wang, T., Zhang, H., Wang, Y., Ding, J., and Tian, X.: Constraint of satellite CO₂ retrieval on the global carbon cycle from a
1109 Chinese atmospheric inversion system, *Sci. China Earth Sci.*, 66, 609–618, 2023.

1110 Jones, M. W., Andrew, R. M., Peters, G. P., Janssens-Maenhout, G., De-Gol, A. J., Dou, X., Liu, Z., Pickers, P., Ciais, P., Patra, P. K.,
1111 Chevallier, F., and Le Quéré, C.: Gridded fossil CO₂ emissions and related O₂ combustion consistent with national inventories,
1112 2022.

1113 Kaminski, T., Rayner, P. J., Heimann, M., and Enting, I. G.: On aggregation errors in atmospheric transport inversions, *J. Geophys. Res.*
1114 *D: Atmos.*, 106, 4703–4715, 2001.

1115 Klein Goldewijk, K., Beusen, A., Doelman, J., and Stehfest, E.: Anthropogenic land use estimates for the Holocene – HYDE 3.2, *Earth*
1116 *Syst. Sci. Data*, 9, 927–953, 2017.

1117 Kong, Y., Zheng, B., Zhang, Q., and He, K.: Global and regional carbon budget for 2015–2020 inferred from OCO-2 based on an
1118 ensemble Kalman filter coupled with GEOS-Chem, *Atmos. Chem. Phys.*, 22, 10769–10788, 2022.

1119 van der Laan-Luijkx, I. T., van der Velde, I. R., van der Veen, E., Tsuruta, A., Stanislawski, K., Babenhauserheide, A., Zhang, H. F., Liu,
1120 Y., He, W., Chen, H., Masarie, K. A., Krol, M. C., and Peters, W.: The CarbonTracker Data Assimilation Shell (CTDAS) v1.0:
1121 implementation and global carbon balance 2001–2015, *Geosci. Model Dev.*, 10, 2785–2800, 2017.

1122 Lauvaux, T., Giron, C., Mazzolini, M., d’Aspremont, A., Duren, R., Cusworth, D., Shindell, D., and Ciais, P.: Global assessment of oil and
1123 gas methane ultra-emitters, *Science*, 375, 557–561, 2022.

1124 Liu, J., Baskaran, L., Bowman, K., Schimel, D., Bloom, A. A., Parazoo, N. C., Oda, T., Carroll, D., Menemenlis, D., Joiner, J., Commane,
1125 R., Daube, B., Gatti, L. V., McKain, K., Miller, J., Stephens, B. B., Sweeney, C., and Wofsy, S.: Carbon Monitoring System Flux
1126 Net Biosphere Exchange 2020 (CMS-Flux NBE 2020), *Earth System Science Data*, 13, 299–330, 2021.

1127 Maksyutov, S., Oda, T., Saito, M., Janardanan, R., Belikov, D., Kaiser, J. W., Zhuravlev, R., Ganshin, A., Valsala, V. K., Andrews, A.,
1128 Chmura, L., Dlugokencky, E., Haszpra, L., Langenfelds, R. L., Machida, T., Nakazawa, T., Ramonet, M., Sweeney, C., and Worthy,
1129 D.: Technical note: A high-resolution inverse modelling technique for estimating surface CO₂ fluxes based on the NIES-TM–
1130 FLEXPART coupled transport model and its adjoint, *Atmos. Chem. Phys.*, 21, 1245–1266, 2021.

1131 Mason Earles, J., Yeh, S., and Skog, K. E.: Timing of carbon emissions from global forest clearance, *Nat. Clim. Chang.*, 2, 682–685, 2012.

1132 Mayorga, E., Seitzinger, S. P., Harrison, J. A., Dumont, E., Beusen, A. H. W., Bouwman, A. F., Fekete, B. M., Kroeze, C., and Van
1133 Drecht, G.: Global Nutrient Export from WaterSheds 2 (NEWS 2): Model development and implementation, *Environmental*
1134 *Modelling & Software*, 25, 837–853, 2010.

1135 Naus, S., Domingues, L. G., Krol, M., Lujkx, I. T., Gatti, L. V., Miller, J. B., Gloor, E., Basu, S., Correia, C., Koren, G., Worden, H. M.,
1136 Flemming, J., Pétron, G., and Peters, W.: Sixteen years of MOPITT satellite data strongly constrain Amazon CO fire emissions,
1137 *Atmos. Chem. Phys.*, 22, 14735–14750, 2022.

1138 Niwa, Y., Ishijima, K., Ito, A., and Iida, Y.: Toward a long-term atmospheric CO₂ inversion for elucidating natural carbon fluxes:
1139 technical notes of NISMON-CO₂ v2021.1, *Progress in Earth and Planetary Science*, 9, 1–19, 2022.

1140 Ogle, S. M., Domke, G., Kurz, W. A., Rocha, M. T., Huffman, T., Swan, A., Smith, J. E., Woodall, C., and Krug, T.: Delineating managed

1141 land for reporting national greenhouse gas emissions and removals to the United Nations framework convention on climate change,
1142 Carbon Balance Manag., 13, 9, 2018.

1143 Patra, P. K., Takigawa, M., Watanabe, S., Chandra, N., Ishijima, K., and Yamashita, Y.: Improved Chemical Tracer Simulation by
1144 MIROC4.0-based Atmospheric Chemistry-Transport Model (MIROC4-ACTM), SOLAIAT, 14, 91–96, 2018.

1145 Patra, P. K., Dlugokencky, E. J., Elkins, J. W., Dutton, G. S., Tohjima, Y., Sasakawa, M., Ito, A., Weiss, R. F., Manizza, M., Krummel, P.
1146 B., Prinn, R. G., O’doherly, S., Bianchi, D., Nevison, C., Solazzo, E., Lee, H., Joo, S., Kort, E. A., Maity, S., and Takigawa, M.:
1147 Forward and Inverse Modelling of Atmospheric Nitrous Oxide Using MIROC4-Atmospheric Chemistry-Transport Model, Journal of
1148 the Meteorological Society of Japan. Ser. II, 100, 361–386, 2022.

1149 Peng, S., Lin, X., Thompson, R. L., Xi, Y., Liu, G., Hauglustaine, D., Lan, X., Poulter, B., Ramonet, M., Saunois, M., Yin, Y., Zhang, Z.,
1150 Zheng, B., and Ciais, P.: Wetland emission and atmospheric sink changes explain methane growth in 2020, Nature, 612, 477–482,
1151 2022.

1152 Perugini, L., Pellis, G., Grassi, G., Ciais, P., Dolman, H., House, J. I., Peters, G. P., Smith, P., Günther, D., and Peylin, P.: Emerging
1153 reporting and verification needs under the Paris Agreement: How can the research community effectively contribute?, Environ. Sci.
1154 Policy, 122, 116–126, 2021.

1155 Petrescu, A. M. R., McGrath, M. J., Andrew, R. M., Peylin, P., Peters, G. P., Ciais, P., Broquet, G., Tubiello, F. N., Gerbig, C., Pongratz,
1156 J., Janssens-Maenhout, G., Grassi, G., Nabuurs, G.-J., Regnier, P., Lauerwald, R., Kuhnert, M., Balkovič, J., Schelhaas, M.-J., Denier
1157 van der Gon, H. A. C., Solazzo, E., Qiu, C., Pilli, R., Kononov, I. B., Houghton, R. A., Günther, D., Perugini, L., Crippa, M.,
1158 Ganzenmüller, R., Luijkx, I. T., Smith, P., Munassar, S., Thompson, R. L., Conchedda, G., Monteil, G., Scholze, M., Karstens, U.,
1159 Brockmann, P., and Dolman, A. J.: The consolidated European synthesis of CO₂ emissions and removals for the European Union
1160 and United Kingdom: 1990–2018, Earth Syst. Sci. Data, 13, 2363–2406, 2021.

1161 Philibert, A., Loyce, C., and Makowski, D.: Prediction of N₂O emission from local information with Random Forest, Environ. Pollut.,
1162 177, 156–163, 2013.

1163 Potapov, P., Hansen, M. C., Laestadius, L., Turubanova, S., Yaroshenko, A., Thies, C., Smith, W., Zhuravleva, I., Komarova, A.,
1164 Minnemeyer, S., and Esipova, E.: The last frontiers of wilderness: Tracking loss of intact forest landscapes from 2000 to 2013, Sci
1165 Adv, 3, e1600821, 2017.

1166 Regnier, P., Friedlingstein, P., Ciais, P., Mackenzie, F. T., Gruber, N., Janssens, I. A., Laruelle, G. G., Lauerwald, R., Luysaert, S.,
1167 Andersson, A. J., Arndt, S., Arnosti, C., Borges, A. V., Dale, A. W., Gallego-Sala, A., Goddérís, Y., Goossens, N., Hartmann, J.,
1168 Heinze, C., Ilyina, T., Joos, F., LaRowe, D. E., Leifeld, J., Meysman, F. J. R., Munhoven, G., Raymond, P. A., Spahni, R.,

1169 Suntharalingam, P., and Thullner, M.: Anthropogenic perturbation of the carbon fluxes from land to ocean, *Nat. Geosci.*, 6, 597–607,
1170 2013.

1171 Rödenbeck, C., Houweling, S., Gloor, M., and Heimann, M.: CO₂ flux history 1982–2001 inferred from atmospheric data using a global
1172 inversion of atmospheric transport, *Atmos. Chem. Phys.*, 3, 1919–1964, 2003.

1173 Saunio, M., Stavert, A. R., Poulter, B., Bousquet, P., Canadell, J. G., Jackson, R. B., Raymond, P. A., Dlugokencky, E. J., Houweling, S.,
1174 Patra, P. K., Ciais, P., Arora, V. K., Bastviken, D., Bergamaschi, P., Blake, D. R., Brailsford, G., Bruhwiler, L., Carlson, K. M.,
1175 Carrol, M., Castaldi, S., Chandra, N., Crevoisier, C., Crill, P. M., Covey, K., Curry, C. L., Etiope, G., Frankenberg, C., Gedney, N.,
1176 Hegglin, M. I., Höglund-Isaksson, L., Hugelius, G., Ishizawa, M., Ito, A., Janssens-Maenhout, G., Jensen, K. M., Joos, F., Kleinen,
1177 T., Krummel, P. B., Langenfelds, R. L., Laruelle, G. G., Liu, L., Machida, T., Maksyutov, S., McDonald, K. C., McNorton, J.,
1178 Miller, P. A., Melton, J. R., Morino, I., Müller, J., Murguia-Flores, F., Naik, V., Niwa, Y., Noce, S., O’Doherty, S., Parker, R. J.,
1179 Peng, C., Peng, S., Peters, G. P., Prigent, C., Prinn, R., Ramonet, M., Regnier, P., Riley, W. J., Rosentreter, J. A., Segers, A.,
1180 Simpson, I. J., Shi, H., Smith, S. J., Steele, L. P., Thornton, B. F., Tian, H., Tohjima, Y., Tubiello, F. N., Tsuruta, A., Viovy, N.,
1181 Voulgarakis, A., Weber, T. S., van Weele, M., van der Werf, G. R., Weiss, R. F., Worthy, D., Wunch, D., Yin, Y., Yoshida, Y.,
1182 Zhang, W., Zhang, Z., Zhao, Y., Zheng, B., Zhu, Q., Zhu, Q., and Zhuang, Q.: The global methane budget 2000–2017, *Earth Syst.*
1183 *Sci. Data*, 12, 1561–1623, 2020.

1184 Saunio, M., Martinez, A., Poulter, B., Zhang, Z., Raymond, P., Regnier, P., Canadell, J. G., Jackson, R. B., Patra, P. K., Bousquet, P.,
1185 Ciais, P., Dlugokencky, E. J., Lan, X., Allen, G. H., Bastviken, D., Beerling, D. J., Belikov, D. A., Blake, D. R., Castaldi, S., Crippa,
1186 M., Deemer, B. R., Dennison, F., Etiope, G., Gedney, N., Höglund-Isaksson, L., Holgerson, M. A., Hopcroft, P. O., Hugelius, G., Ito,
1187 A., Jain, A. K., Janardanan, R., Johnson, M. S., Kleinen, T., Krummel, P., Lauerwald, R., Li, T., Liu, X., McDonald, K. C., Melton,
1188 J. R., Mühle, J., Müller, J., Murguia-Flores, F., Niwa, Y., Noce, S., Pan, S., Parker, R. J., Peng, C., Ramonet, M., Riley, W. J.,
1189 Rocher-Ros, G., Rosentreter, J. A., Sasakawa, M., Segers, A., Smith, S. J., Stanley, E. H., Thanwerdas, J., Tian, H., Tsuruta, A.,
1190 Tubiello, F. N., Weber, T. S., van der Werf, G., Worthy, D. E., Xi, Y., Yoshida, Y., Zhang, W., Zheng, B., Zhu, Q., Zhu, Q., and
1191 Zhuang, Q.: Global Methane Budget 2000–2020, *Earth Syst. Sci. Data Discuss.* [preprint], <https://doi.org/10.5194/essd-2024-115>, in
1192 review, 2024.

1193 Schuldt, K. N., Mund, J., Luijkx, I. T., Aalto, T., Abshire, J. B., Aikin, K., Andrews, A., Aoki, S., Apadula, F., Baier, B., Bakwin, P.,
1194 Bartyzel, J., Bentz, G., Bergamaschi, P., Beyersdorf, A., Biermann, T., Biraud, S. C., Boenisch, H., Bowling, D., Brailsford, G., van
1195 den Bulk, P., Chen, G., Chen, H., Chmura, L., Clark, S., Climadat, S., Della Coletta, J., Colomb, A., Commane, R., Conil, S., Cox,
1196 A., Cristofanelli, P., Cuevas, E., Curcoll, R., Daube, B., Davis, K., Delmotte, M., DiGangi, J. P., van Dinter, D., Dlugokencky, E.,

1197 Elkins, J. W., Emmenegger, L., Fang, S., Fischer, M. L., Forster, G., Frumau, A., Galkowski, M., Gatti, L. V., Gehrlein, T., Gerbig,
1198 C., Gheusi, F., Gloor, E., Gomez-Trueba, V., Goto, D., Griffis, T., Hammer, S., Hanson, C., Haszpra, L., Hatakka, J., Heimann, M.,
1199 Heliasz, M., Hensen, A., Hermanssen, O., Hintsä, E., Holst, J., Ivakhov, V., Jaffe, D., Joubert, W., Karion, A., Kawa, S. R., Kazan,
1200 V., Keeling, R., Keronen, P., Kolari, P., Kominkova, K., Kort, E., Kozlova, E., Krummel, P., Kubistin, D., Labuschagne, C., Lam, D.
1201 H. Y., Langenfelds, R., Laurent, O., Laurila, T., Lauvaux, T., Lavric, J., Law, B., Lee, J., Lee, O. S. M., Lehner, I., Leppert, R.,
1202 Leuenberger, M., Levin, I., Levula, J., Lin, J., Lindauer, M., Loh, Z., Lopez, M., Machida, T., et al.: Multi-laboratory compilation of
1203 atmospheric carbon dioxide data for the period 1957-2020; obspack_co2_1_GLOBALVIEWplus_v7.0_2021-08-18, 2021.

1204 Schuldt, K. N., Jacobson, A. R., Aalto, T., Andrews, A., Bakwin, P., Bergamaschi, P., Biermann, T., Biraud, S. C., Chen, H., Colomb, A.,
1205 Conil, S., Cristofanelli, P., Delmotte, M., Dlugokencky, E., Emmenegger, L., Fischer, M. L., Hatakka, J., Heliasz, M., Hermanssen,
1206 O., Holst, J., Jaffe, D., Karion, A., Kazan, V., Keronen, P., Kominkova, K., Kubistin, D., Laurent, O., Laurila, T., Lee, J., Lehner, I.,
1207 Leuenberger, M., Lindauer, M., Lopez, M., Mammarella, I., Manca, G., Marek, M. V., De Mazière, M., McKain, K., Miller, C. E.,
1208 Miller, J. B., Mölder, M., Müller-Williams, J., Myhre, C. L., Piacentino, S., Pichon, J. M., Plass-Duelmer, C., Plass-Duelmer, C.,
1209 Ramonet, M., di Sarra, A. G., Scheeren, B., Schumacher, M., Sha, M. K., Sloop, C. D., Smith, P., Steinbacher, M., Sweeney, C.,
1210 Tans, P., Thoning, K., Tørseth, K., Trisolino, P., Viner, B., Vitkova, G., and De Wekker, S.: Multi-laboratory compilation of
1211 atmospheric carbon dioxide data for the year 2022; obspack_co2_1_NRT_v7.2_2022-06-28, 2022.

1212 Segers, A. and Houweling, S.: Description of the CH₄ Inversion Production Chain, Copernicus Atmosphere Monitoring Service, 2017.

1213 Shcherbak, I., Millar, N., and Robertson, G. P.: Global metaanalysis of the nonlinear response of soil nitrous oxide (N₂O) emissions to
1214 fertilizer nitrogen, *Proc. Natl. Acad. Sci. U. S. A.*, 111, 9199–9204, 2014.

1215 Thompson, R. L., Chevallier, F., Crotwell, A. M., Dutton, G., Langenfelds, R. L., Prinn, R. G., Weiss, R. F., Tohjima, Y., Nakazawa, T.,
1216 Krummel, P. B., Steele, L. P., Fraser, P., O’Doherty, S., Ishijima, K., and Aoki, S.: Nitrous oxide emissions 1999 to 2009 from a
1217 global atmospheric inversion, *Atmos. Chem. Phys.*, 14, 1801–1817, 2014.

1218 Tian, H., Yang, J., Xu, R., Lu, C., Canadell, J. G., Davidson, E. A., Jackson, R. B., Arneth, A., Chang, J., Ciais, P., Gerber, S., Ito, A.,
1219 Joos, F., Lienert, S., Messina, P., Olin, S., Pan, S., Peng, C., Saikawa, E., Thompson, R. L., Vuichard, N., Winiwarter, W., Zaehle, S.,
1220 and Zhang, B.: Global soil nitrous oxide emissions since the preindustrial era estimated by an ensemble of terrestrial biosphere
1221 models: Magnitude, attribution, and uncertainty, *Glob. Chang. Biol.*, 25, 640–659, 2019.

1222 Tian, H., Xu, R., Canadell, J. G., Thompson, R. L., Winiwarter, W., Suntharalingam, P., Davidson, E. A., Ciais, P., Jackson, R. B.,
1223 Janssens-Maenhout, G., Prather, M. J., Regnier, P., Pan, N., Pan, S., Peters, G. P., Shi, H., Tubiello, F. N., Zaehle, S., Zhou, F.,
1224 Arneth, A., Battaglia, G., Berthet, S., Bopp, L., Bouwman, A. F., Buitenhuis, E. T., Chang, J., Chipperfield, M. P., Dangal, S. R. S.,

1225 Dlugokencky, E., Elkins, J. W., Eyre, B. D., Fu, B., Hall, B., Ito, A., Joos, F., Krummel, P. B., Landolfi, A., Laruelle, G. G.,
1226 Lauerwald, R., Li, W., Lienert, S., Maavara, T., MacLeod, M., Millet, D. B., Olin, S., Patra, P. K., Prinn, R. G., Raymond, P. A.,
1227 Ruiz, D. J., van der Werf, G. R., Vuichard, N., Wang, J., Weiss, R. F., Wells, K. C., Wilson, C., Yang, J., and Yao, Y.: A
1228 comprehensive quantification of global nitrous oxide sources and sinks, *Nature*, 586, 248–256, 2020.

1229 Tian, H., Pan, N., Thompson, R. L., Canadell, J. G., Suntharalingam, P., Regnier, P., Davidson, E. A., Prather, M., Ciais, P., Muntean, M.,
1230 Pan, S., Winiwarter, W., Zaehle, S., Zhou, F., Jackson, R. B., Bange, H. W., Berthet, S., Bian, Z., Bianchi, D., Bouwman, A. F.,
1231 Buitenhuis, E. T., Dutton, G., Hu, M., Ito, A., Jain, A. K., Jeltsch-Thömmes, A., Joos, F., Kou-Giesbrecht, S., Krummel, P. B., Lan,
1232 X., Landolfi, A., Lauerwald, R., Li, Y., Lu, C., Maavara, T., Manizza, M., Millet, D. B., Mühle, J., Patra, P. K., Peters, G. P., Qin, X.,
1233 Raymond, P., Resplandy, L., Rosentreter, J. A., Shi, H., Sun, Q., Tonina, D., Tubiello, F. N., van der Werf, G. R., Vuichard, N.,
1234 Wang, J., Wells, K. C., Western, L. M., Wilson, C., Yang, J., Yao, Y., You, Y., and Zhu, Q.: Global Nitrous Oxide Budget 1980–
1235 2020, *Earth System Science Data Discussions*, 1–98, 2023.

1236 Tibrewal, K., Ciais, P., Saunois, M., Martinez, A., Lin, X., Thanwerdas, J., Deng, Z., Chevallier, F., Giron, C., Albergel, C., Tanaka, K.,
1237 Patra, P., Tsuruta, A., Zheng, B., Belikov, D., Niwa, Y., Janardanan, R., Maksyutov, S., Segers, A., Tzompa-Sosa, Z. A., Bousquet,
1238 P., and Sciare, J.: Assessment of methane emissions from oil, gas and coal sectors across inventories and atmospheric inversions,
1239 *Commun. Earth Environ.*, 5, <https://doi.org/10.1038/s43247-023-01190-w>, 2024.

1240 Tsuruta, A., Aalto, T., Backman, L., Hakkarainen, J., van der Laan-Luijckx, I. T., Krol, M. C., Spahni, R., Houweling, S., Laine, M.,
1241 Dlugokencky, E., Gomez-Pelaez, A. J., van der Schoot, M., Langenfelds, R., Ellul, R., Arduini, J., Apadula, F., Gerbig, C., Feist, D.
1242 G., Kivi, R., Yoshida, Y., and Peters, W.: Global methane emission estimates for 2000–2012 from CarbonTracker Europe-CH4 v1.0,
1243 *Geosci. Model Dev.*, 10, 1261–1289, 2017.

1244 UNFCCC: Biennial Update Report submissions from Non-Annex I Parties, available at: <https://unfccc.int/BURs>, last access: 2 July 2021a.

1245 UNFCCC: National Communication submissions from Non-Annex I Parties, available at: <https://unfccc.int/non-annex-I-NCs>, last access:
1246 5 December 2021b.

1247 Wang, J. A., Baccini, A., Farina, M., Randerson, J. T., and Friedl, M. A.: Disturbance suppresses the aboveground carbon sink in North
1248 American boreal forests, *Nat. Clim. Chang.*, 11, 435–441, 2021.

1249 Wang, Q., Zhou, F., Shang, Z., Ciais, P., Winiwarter, W., Jackson, R. B., Tubiello, F. N., Janssens-Maenhout, G., Tian, H., Cui, X.,
1250 Canadell, J. G., Piao, S., and Tao, S.: Data-driven estimates of global nitrous oxide emissions from croplands, *Natl Sci Rev*, 7, 441–
1251 452, 2020.

1252 van Wees, D., van der Werf, G. R., Randerson, J. T., Rogers, B. M., Chen, Y., Veraverbeke, S., Giglio, L., and Morton, D. C.: Global

1253 biomass burning fuel consumption and emissions at 500 m spatial resolution based on the Global Fire Emissions Database (GFED),
1254 Geoscientific Model Development, 15, 8411–8437, 2022.

1255 Wells, K. C., Millet, D. B., Bousseres, N., Henze, D. K., Chaliyakunnel, S., Griffis, T. J., Luan, Y., Dlugokencky, E. J., Prinn, R. G.,
1256 O’Doherty, S., Weiss, R. F., Dutton, G. S., Elkins, J. W., Krummel, P. B., Langenfelds, R., Steele, L. P., Kort, E. A., Wofsy, S. C.,
1257 and Umezawa, T.: Simulation of atmospheric N₂O with GEOS-Chem and its adjoint: evaluation of observational constraints, Geosci.
1258 Model Dev., 8, 3179–3198, 2015.

1259 Wilson, C., Chipperfield, M. P., Gloor, M., and Chevallier, F.: Development of a variational flux inversion system (INVICAT v1.0) using
1260 the TOMCAT chemical transport model, Geosci. Model Dev., 7, 2485–2500, 2014.

1261 Winkler, K., Yang, H., Ganzenmüller, R., Fuchs, R., Ceccherini, G., Duveiller, G., Grassi, G., Pongratz, J., Bastos, A., Shvidenko, A.,
1262 Araza, A., Herold, M., Wigneron, J.-P., and Ciais, P.: Changes in land use and management led to a decline in Eastern Europe’s
1263 terrestrial carbon sink, Communications Earth & Environment, 4, 1–14, 2023.

1264 Xu, X., Sharma, P., Shu, S., Lin, T.-S., Ciais, P., Tubiello, F. N., Smith, P., Campbell, N., and Jain, A. K.: Global Greenhouse Gas
1265 Emissions from Plant-and Animal-Based Food, Nature Food, 2021.

1266 Yao, Y., Tian, H., Shi, H., Pan, S., Xu, R., Pan, N., and Canadell, J. G.: Increased global nitrous oxide emissions from streams and rivers
1267 in the Anthropocene, Nat. Clim. Chang., 10, 138–142, 2019.

1268 Yin, Y., Chevallier, F., Ciais, P., Broquet, G., Fortems-Cheiney, A., Pison, I., and Saunois, M.: Decadal trends in global CO emissions as
1269 seen by MOPITT, Atmos. Chem. Phys., 15, 13433–13451, 2015.

1270 Zheng, B., Chevallier, F., Ciais, P., Yin, Y., Deeter, M. N., Worden, H. M., Wang, Y., Zhang, Q., and He, K.: Rapid decline in carbon
1271 monoxide emissions and export from East Asia between years 2005 and 2016, Environ. Res. Lett., 13, 044007, 2018.

1272 Zhou, F., Shang, Z., Zeng, Z., Piao, S., Ciais, P., Raymond, P. A., Wang, X., Wang, R., Chen, M., Yang, C., Tao, S., Zhao, Y., Meng, Q.,
1273 Gao, S., and Mao, Q.: New model for capturing the variations of fertilizer-induced emission factors of N₂O, Global Biogeochem.
1274 Cycles, 29, 885–897, 2015.

1275 Zscheischler, J., Mahecha, M. D., Avitabile, V., Calle, L., Carvalhais, N., Ciais, P., Gans, F., Gruber, N., Hartmann, J., Herold, M., Ichii,
1276 K., Jung, M., Landschützer, P., Laruelle, G. G., Lauerwald, R., Papale, D., Peylin, P., Poulter, B., Ray, D., Regnier, P., Rödenbeck,
1277 C., Roman-Cuesta, R. M., Schwalm, C., Tramontana, G., Tyukavina, A., Valentini, R., van der Werf, G., West, T. O., Wolf, J. E.,
1278 and Reichstein, M.: Reviews and syntheses: An empirical spatiotemporal description of the global surface–atmosphere carbon fluxes:
1279 opportunities and data limitations, Biogeosciences, 14, 3685–3703, 2017.

1280

1281

1282